Widely spaced wave-particle observations during GEOTAIL and Wind magnetic conjunctions in the Earth's ion foreshock with near-radial interplanetary magnetic field

D. Berdichevsky,[1] G. Thejappa,[2] R.J. Fitzenreiter,[3] R.L. Lepping,[3] T. Yamamoto,[4] S. Kokubun,[5] R.W. McEntire,[6] D.J. Williams,[6] and R.P. Lin[7]

Abstract. Several events have been identified of an ion foreshock extending up to 250 RE upstream of the Earth. These events occur mostly during periods of slowly drifting radial interplanetary magnetic field (IMF) when the 1-min average values of the strengths of the IMF and the solar wind (SW) speeds are mostly steady. For their analysis an analytical solution to the problem of the closest approach of an IMF line to two spacecraft is given. We used this method to find intervals of magnetic conjunction between the bow shock and the upstream regions at GEOTAIL and Wind. This solution is obtained by determining the minimum angle θ (as a function of time) between the mean direction of the IMF (measured at Wind) and the vector-difference ($r_{WI}-r$) of the locations of Wind and the point (attached on the field line) which went earlier by GEOTAIL. Here we take into account the mean drift of the flux lines with the SW, by assuming that the spacecraft were located in the same heliospheric magnetic domain. We have tested this method against a set of selected cases which show a steady presence of the ion foreshock close to the bow shock (GEOTAIL) and its sporadic presence far upstream (Wind). We have found our method to be accurate within a few Earth radii (RE). We have identified an outstanding candidate for the bow shock, GEOTAIL, and Wind sequential magnetic conjunction, which occurred on June 11, 1995. Additionally, this diagnostic technique has been applied to nine more intervals of simultaneous occurrences of intensity enhancements of broadband ultralow-frequency (ULF) waves, and fluctuating fluxes of scattered energetic ions (40-140 keV). Very broad ion foreshock regions (> 40 RE) are commonly observed during the subset of events characterized by a high-speed SW. The observed frequencies of the ULF waves are basically enhanced transversal modes in the range from ~ 1/10 to 2/3 of proton cyclotron frequency, f_{cp}. Fluctuations in the energetic ion fluxes were also observed in this frequency range for all the cases. Therefore we argue that the nature of the coupling between ULF waves and energetic ions is similar both in the near as well as far upstream regions of the Earth's bow shock.

1. Introduction

Upstreaming ions with energy a few times greater than the energy of the ambient solar wind (SW) protons near and far from the bow shock were reported in the pioneering work of *Asbridge et al.* [1968]. Magnetometer observations [*Heppner et al.*, 1967; *Greenstadt et al.*, 1968] indicated the occurrence of large-amplitude 0.01-0.05 Hz waves in the same regions. *Fairfield* [1969] identified these low frequency fluctuations as

[1]Raytheon-STX Corporation, at NASA/GSFC, Greenbelt, MD 20771, email: berdi@istp1.gsfc.nasa.gov.

[2]Dept. of Astr., Univ. of Maryland, College Park, MD 20742

[3]NASA/GSFC, Greenbelt, MD 20771

[4]Instiue of Space and Astronautical Science, Sagamihara, Kanagawa 229, Japan

[5]Solar-Terrestrial Environment Laboratory, Nagoya University, Toyokawa, Aichi 442, Japan

[6] JHU/Appplied Physics Laboratory, Laurel, MD

[7] Dept. of Phys., Univ. of California, Berkeley, CA

Alfvèn waves. Fairfield argued that since these waves cannot move upstream against the SW flow, due to their low characteristic speeds of ~ 50 km s^{-1} at 1 AU which is well below the typical SW speed of ~ 400 km s^{-1}, they are most probably excited locally. *Lin et al.* (1974) reported the observations of (30-100 keV) scattered ion populations within 30 Earth radii (RE) upstream from the bow shock, whenever the spacecraft (SC) is connected to the bow shock through interplanetary magnetic field (IMF) lines. Most probably, these observations correspond to quasi-parallel shocks, which are well known for their intricate nature [e.g., *Kennel*, 1981]. This region is usually referred to as the "ion foreshock" in the dayside, i.e., upstream from or laterally close to the nose of the Earth's bow shock within about 15-20 RE from its location. Since the cyclotron radii of the scattered 30-100 keV ions were comparable to the wavelengths of the ULF magnetohydrodynamic wave, *Lin et al.* [1974] argue that most probably a strong coupling between energetic ions and these ULF waves exists. *Gosling et al.* [1978] reported the existence of two distinct populations of energetic upstream ions, namely (1) the scattered ion distributions and (2) the nonscattered field-aligned loss-cone distributions. Large amplitude compressional and transversal magnetic waves were observed in the upstream regions, especially very close to the bow shock, in conjunction with "diffuse" energetic ions (3-40 keV), but not

with the beam like distribution of "reflected" ions [see, e.g., *Paschmann et al.* [1979]. Subsequent intense research in this field helped us to build an overall picture of the morphology and characteristics of the Earth's ion foreshock (e.g., the special section "Upstream Waves and Particles" in Journal of Geophysical Research, 86(A6), 4317-4538, 1981).

The energetic ions analyzed in this study most probably correspond to strongly scattered energetic ion populations. The angular distribution of these energetic ions appears to be similar to the standard distribution of diffuse ions used by *Bonifazi and Moreno* [1981]. An improved analysis of the boundaries of the ion foreshock was possible through the introduction of the ion "solar foreshock coordinates," which are defined in the plane given by the SW velocity and the direction of the IMF (**V-B** plane) (*Greenstadt and Baum*, 1986). This method was also used by *Le and Russell* [1992], which allowed them to identify the ion foreshock boundary more accurately. The diversity of the energetic upstream ion populations and ULF waves in the ion foreshock were observed and discussed in the literature [see, e.g., *Fuselier*, 1995; *Greenstadt et al.*, 1995]. *Terasawa* [1979] advanced models for the scattering of the energetic ions. The coupling of energetic ions with the ULF waves was discussed by *Eichler* [1981] and *Lee* [1982]. Numerical hybrid-particle simulations of collisionless shocks demonstrated the effectiveness of shock drift acceleration in generating a population of backstreaming particles [*Burgess*, 1987]. Diffusion acceleration was used in Monte Carlo shock simulations of the injection of thermal ions, their acceleration at Earth's bow shock, and comparison of observed upstream and downstream events [Ellison et al. 1990].

When the SW flows approximately parallel to the IMF, the foreshock's boundary is ill defined. *Greenstadt and Baum* [1986] and *Le and Russell* [1992] show that the boundary of the ion foreshock is not well resolved for a **V-B** angle smaller than ~ 25°. In such a case several questions remain unanswered, namely; (1) Do strong scattered energetic ions exist in the ion foreshock at hundreds of RE upstream of the bow shock? (2) How does the near upstream ion foreshock region compare with that of the far upstream? And (3) what is the relationship between the large-amplitude ULF waves and the pre-existing SW fluctuations? In this paper we address some of these issues. We present an analytical solution to the problem of the closest approach of an IMF flux line to two spacecraft and show that this solution is valid over reasonable extensions of time and space in the SW. This method allows the determination of time intervals when near and far ion foreshock regions are simultaneously or sequentially connected to neighboring bow shock locations. We use this method in the analysis of the observations of similar ion foreshock conditions such as the enhanced ultralow frequency (ULF) waves and strongly scattered energetic ions in the near (tens of RE) and far upstream regions (hundreds of RE) from the bow shock. In this study we present 10 examples of these events. This study will help us to answer some questions arising in the debate on the origin of the strongly scattered energetic ion population [a few to hundreds of keV] upstream of the ion bow shock.

In this study we use the 3-s average IMF data from the GEOTAIL magnetic field (MGF) experiment [*Kokubun et al.*, 1994]. The 6-s average energetic ion data in the energy range from 61.5-89.7 keV are from the GEOTAIL energetic particles composition (EPIC) instrument, as are the 48-s average fluxes from higher energy channels [*Williams et al.*, 1994]. We also use the Wind magnetic field investigation (MFI) magnetometer 3-second average data [*Lepping et al.*, 1995]. The SW electron data are from the Wind solar wind experiment (SWE) plasma instrument [*Ogilvie et al.*, 1995] and the Wind energetic ion data (40-160 keV) is from the three-dimensional plasma analyzer (3DP) [*Lin et al.*, 1995]. Telemetry constraints result in a flow of 3DP energetic ion fluxes every 12 s when Wind is beyond ≈120 RE, and every 6 s for a Wind within ≈120 RE from the Earth. Therefore the SWE electron data are 3 s snap-shots obtained either every 12 s, or every 6 s.

This paper is organized as follows. Section 2 presents the general features of these widely spaced wave/particle observations of the Earth's ion foreshock. Section 3 presents a method which allows for the straightforward quantitative evaluation of the magnetic conjunction condition between two spacecraft located, near as well as far, upstream from the bow shock. Section 4 describes an especially interesting example which illustrates the common physical characteristics of these ion foreshock events. In Section 5 we analyze in detail the magnetic conjunction condition for two events. Section 6 presents the analysis of ULF wave data corresponding to all events. Section 7 presents the unusually long-lasting observations of IMF at opposite sides of a heliospheric boundary for one event. Section 8 presents the conclusions.

2. General Features of the Widely Spaced Observations of the Ion Foreshock

We present 10 events of intensity enhancements in ULF waves and energetic particles observed in the far Earth's ion-foreshock by Wind and in the near ionforeshock by GEOTAIL. The technique used to identify these time intervals is given in the appendix. Figure 1 schematically illustrates general conditions of these events. We show in Figure 1 "1" the mean direction of the IMF (**B**) is nearly-parallel to the SW velocity (V_{SW}), and the direction of the drift velocity u_{dr} of the frozen field lines is approximately perpendicular to V_{SW}, "2" approximately isotropic populations of energetic ions (bow shock rest frame of reference) and very intense broadbanded ULF B field wave activity within 20 RE from the Earth's bow shock, and "3" a strongly scattered population of 40 to 140 keV ions, and enhanced broadbanded ULF B field wave activity in the far ion foreshock regions, i.e., ≈ 70-230 RE upstream of the Earth's bow shock. Question marks at the bottom in Figure 1 indicate our limited knowledge of the foreshock boundaries for an approximately radial IMF. The statistical representation of the bow shock in Figure 1 is from *Peredo et al.* [1995, equation 7] for an Alfvénic Mach number ~ 10. The statistical bow shock fit relies on data which reach downstream up to x-GSE ≈ − 40 RE from Earth. Hence its extension beyond − 40 RE is in question, especially for an IMF nearly parallel to the SW. During several of these events Wind appeared to crisscross the electron foreshock from a few minutes to 1 hour or longer before the strong scattered energetic ions were observed.

The spacecraft configurations during the events are similar to those reported by *Mitchell et al.* [1983] and *Scholer et al.* [1980], where the IMF direction was very close to being radial from the Sun. For other studies of the energetic ions in the far ion foreshock we refer to *Sanderson et al.* [1981]. During these SC configurations, nearly isotropic distributions of energetic upstream ions in the SC frame of reference at 30 RE or less from
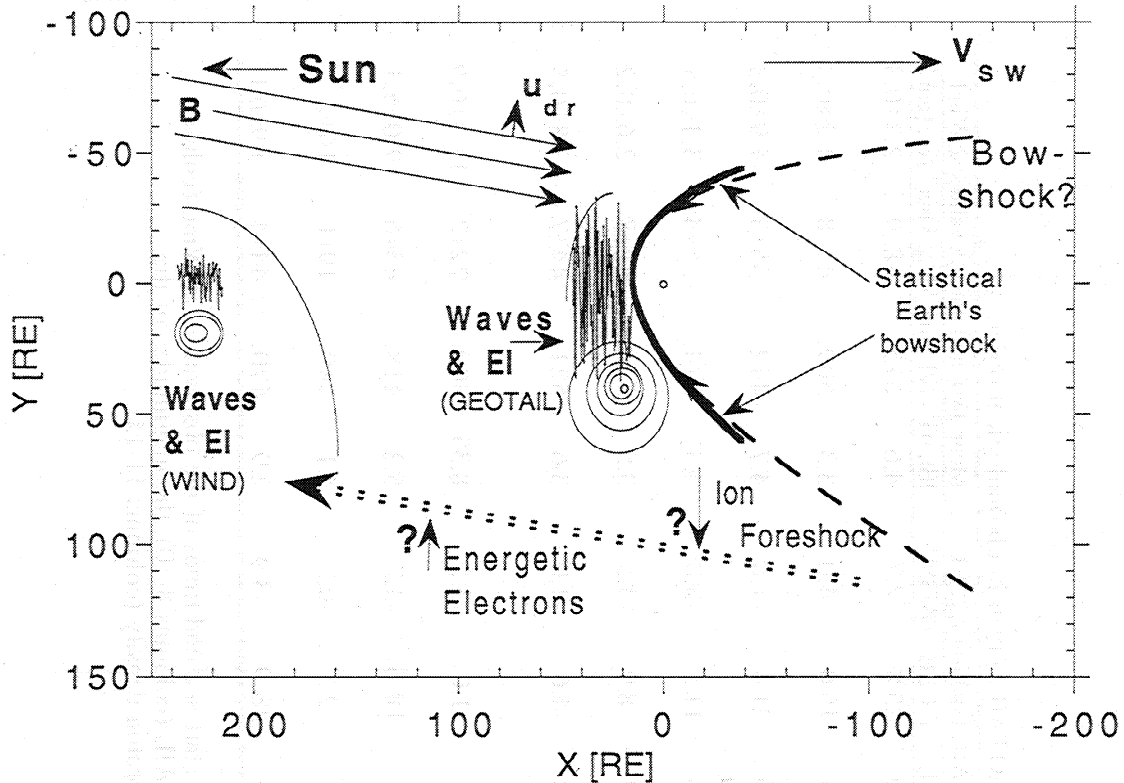
Figure 1. Sketch of the conditions of the far and close Earth ion foreshocks during near-parallel interplanetary magnetic field (IMF) to the flow of the solar wind (SW), corresponding to the events presented in this work. The top presents the direction to the Sun, the direction of the SW, and orientation of the convection velocity for the sketched near-parallel orientation of the IMF to the SW. Regions of the simultaneous observation of ULF wave (sketched using actual 3-s average IMF data) and strongly scattered energetic ions (EI) (sketched with concentric ellipses, suggesting the upstreaming ion population) are drawn in the middle. The thick solid curve gives the location of the statistical bow shock derived by *Peredo et al.*, [1995]. This representation of the bow shock corresponds to a SW along the x axis, its origin is centered at Earth (indicated with an open circle), and uses a modified geocentric solar ecliptic (GSE) coordinate system. The long-dashed curve indicates the possible extension of the bow shock far downstream from Earth's location. In the bottom a double short-dashed-arrowed line and question marks suggest the possible boundaries in the SW of the foreshock.

the bow shock were reported [Scholer et al., 1979], which is consistent with the scenario of negligible convection of the energetic ions by the SW.

In Table 1 we order the events chronologically and present information on the location of Wind and GEOTAIL spacecraft at the time of each event. Table 1 also provides a synthesis of the mean SW conditions during these 10 identified conjunction events. It can be seen from the last four columns that the examples presented in this table cover a range of SW conditions. For example, the mean SW velocity $<V>$, plasma density $<N>$, and H^+ thermal speed $<V_{th}>$ vary from 700 to 300 km s^{-1}, 16 to 2 particles per cubic centimeter, and 50 to 20 km s^{-1}, respectively.

In Table 2 we present the conditions of geometrical magnetic conjunction given by IMF lines and SW velocity at Wind. A closer look at Table 2 suggests a more extended ion foreshock for higher SW stream speeds ($<V> \geq 500$ km s^{-1}). As seen from Table 2, Wind appears to be located inside the ion foreshock region, when a ray along the direction of the mean $<B>$, at Wind, is within 50 RE of the location of the vector position of the bow shock subsolar point r_{sp}. (In the

geocentric solar ecliptic (GSE) coordinate system $r_{sp} \approx$ (14.,0,0) RE, for average SW conditions; see *Peredo et al.* [1995, Table 2]. Table 2 –this work– also shows that at lower SW stream speeds ($<V> \leq 400$ km s^{-1}) the far upstream ion foreshock was sighted by Wind when the distance from the imaginary line along the direction of the mean $<B>$, at Wind, was within 30 RE of the location of r_{sp}. For these events the mean distance of GEOTAIL ($<d_{GE}>$) from the ray along the mean IMF $<B>$, at Wind, varied from 60. to 14. RE (see Table 2). For the first eight events the mean direction $<B>$ was within ~20° or less of the direction along the Sun-Earth line. For the last two events the angle between $<B>$ and the direction of the Sun-Earth line were within 30° and 35°, respectively.

For the first eight events in Table 2 the angle between the mean IMF and the direction of the SW flow was close to or smaller than ~10°. For this angle the IMF will be tangent to the bow shock in the nightside, possibly far downstream of the region of validity of the statistical model of the bow shock [*Peredo et al.*, 1995; *Slavin et al.*, 1984], sketched in Figure 1. Event 10 corresponds to a case where Wind and GEOTAIL are located in IMF domains of opposite polarity.

Table 1. Cases of simultaneous observation of energetic ions (EI), by Wind and GEOTAIL, given in chronological order.

Event	Date in 1995	Wind Time [UT]	GEOTAIL Time [UT]	Wind Position r_{WI}, RE			GEOTAIL Position r_{GE}, RE			Mean IMF and plasma values at Wind			
				X GSE	Y GSE	Z GSE	X GSE	Y GSE	Z GSE	|B|, nT	|V|, kms^{-1}	V_{th}, kms^{-1}	N_p, [cm^{-3}]
1	May 5	2124-2230	2156-2305	242.2	46.1	0.9	5.0	25.8	-2.7	4.6	675.	48±9	2.3±0.3
2	May 9	1400-1518	1415-1615	243.4	40.8	-1.3	25.5	15.0	-4.0	3.3	509.	47±8	4.2±0.3
3	May 27	1330-1424	1415-1509	246.1	8.1	-11.3	7.0	21.4	-1.8	4.7	442.	35±5	4.9±0.3
4	June 11	1500-1730	1430-1630	235.5	-17.5	-16.8	27.6	11.5	-3.8	4.3	374.	35±4	3.1±0.5
5	June 22	1100-1242	11:15-12:45	222.3	-31.0	-18.2	27.9	8.9	-3.5	3.5	556.	42±8	2.6±0.2
6	June 26 June 27	2300-2400 0000-0145	2340-2400 0000-0240	214.9	-33.0	-18.0	29.8	-4.6	-4.0	3.6	521.	44±7	3.8±0.5
7	July 13	2024-2200	1900-2225	168.0	-21.1	-17.1	29.4	-1.0	-3.5	8.35	309.	22±2	11.3±0.9
8	Aug. 25	1300-1630	1310-1705	70.7	-30.8	-5.7	22.5	-18.6	-3.2	5.2	418.	45±6	9.0±0.5
9	Aug. 26	2130-2230	2140-2235	80.1	-27.1	-7.2	19.6	2.5	-0.3	4.1	349.	19±1	16±2
10	Sept. 9	1924-2005	1940-2040	82.6	24.9	-10.9	6.0	-28.9	-3.9	2.9	470.	44±4	1.9±0.1

Table 1 gives from left to right the order of the events (column 1), date (column 1), start and end times of the observation at Wind (column 2), same for GEOTAIL (column 3), location of Wind (columns 5-7) and of GEOTAIL (columns 8-10), the magnitudes of the interplanetary magnetic field (IMF), solar wind (SW) velocity, thermal speed, and proton density (columns 11-14).

Table 2. Conditions of geometrical magnetic conjunction given by IMF and SW velocity at Wind.

Event	MEAN IMF at Wind nT			SW Velocity at Wind kms^{-1}			Cosine angle and distance of ray along <B>, at Wind, to the Sonic Point and GEOTAIL.				Convection velocity RE /min		
							Sonic Point		GEOTAIL				
	Bx GSE	By GSE	Bz GSE	Vx GSE	Vy GSE	Vz GSE	$\frac{r_{WI-sp}\,\mathbf{B}}{\lvert r_{WI-sp}\rvert\lvert B\rvert}$	dist. [RE]	$\frac{r_{WI-GE}\,\mathbf{B}}{\lvert r_{WI-GE}\rvert\lvert B\rvert}$	dist. [RE]	$udr(x)$	$udr(y)$	$udr(z)$
1	4.43	0.47	-1.00	-675±12	4±14	-22±16	0.971	56	0.972	56	-0.420	0.667	-1.546
2	3.27	0.43	-0.53	-509±6	-4±14	-22±16	0.987	37	0.985	37.6	-0.227	0.562	-0.946
3	-4.56	0.49	1.06	-442±4	3±13	-9±6	-0.974	52	-.981	46.3	-0.272	-0.389	-0.988
4	-4.26	0.06	-0.12	-374±1	13±8	-8±7	-0.996	21	-.988	32.2	0.0004	0.0727	0.0239
5	-3.50	-0.36	0.14	-556±8	21±19	6±11	-0.968	53	-0.953	60	-0.081	0.727	-0.1495
6	3.42	-0.96	0.38	-521±19	21±15	5±9	0.975	43	0.976	40.6	-0.455	1.445	-0.447
7	-7.85	2.67	0.99	-309±2	16±3	0±2	-0.982	29.6	-0.9855	24	-0.293	-0.739	-0.330
8	-5.16	0.30	-0.77	-418±3	19±5	4±3	-0.880	22.8	-0.963	13.7	-0.094	-0.044	0.610
9	-3.49	1.23	1.70	-349±2	6±2	-1±7	-0.945	23.5	-0.9404	23	-0.860	-0.797	-1.190
10	2.34	1.66	0.04	-470±6	5±9	20±5	0.951	22.7	0.9855	16	-1.505	2.116	0.238

All parameter are in geocentric solar ecliptic, GSE, coordinate system [Russell, 1971]. Columns 1 to 14 contain respectively the event number, components of the IMF and SW velocity at Wind, the cosine of the angle between the location difference of Wind and the nominal sonic position ($\mathbf{r}_{sp}$=(14,,0,0) RE) at the bow shock and the ray along the direction of the mean IMF (evaluated at Wind), the distance of the $\mathbf{r}_{sp}$ from the ray direction along the mean IMF at Wind, the cosine of the angle between the location difference of Wind and GEOTAIL positions and the direction of the mean IMF (evaluated at Wind), distance of GEOTAIL from the direction along the mean IMF at Wind, and the three components of the drift velocity of the field flux lines in the SW.

3. Quantitative Evaluation of the Magnetic Conjunction Conditions

A quantitative evaluation of the magnetic conjunction conditions between two far apart locations in the SW would allow a better understanding of the relationship between the corresponding observations of the ion foreshock. Consequently, we investigate in what sequence Wind and GEOTAIL approach magnetic conjunction for the time intervals presented in Table 1. First, we determine the distance between Wind and the line along the magnetic field at time t, which was, for example, connecting GEOTAIL and the bow shock at time t_0. We illustrate this in the form of a sketch in Figure 2, where we show the locations of GEOTAIL and Wind with respect to the bow shock and the displacement of one of the IMF lines connected to a three dimensional bow shock. We define the mean drift velocity of the frozen-in IMF guiding centers perpendicular to $<B>$ as

$$<u_{dr}> = <V> - (<V> \cdot <B>) <B>/<B>^2.$$

(this is equivalent to $<B> \times (<V> \times <B>)/<B>^2$).

We evaluate $<u_{dr}>$ for the mean IMF ($<B>$) and solar wind parameters at Wind. This is used to find the closest approach of a sliding flux line drifting with constant velocity $<u_{dr}>$ between GEOTAIL (position r_{GE}) and a point of closest approach to Wind, with spatial location r_{WI}. If we know the time t_0, when the magnetic field line connects the GEOTAIL spacecraft to the bow shock, we can follow it until the time t of the closest approach of the same field line to Wind. We determine the time difference $\Delta t = t - t_0$ by taking the scalar product of vector $<B>$ (constant in time) and $X(t)$. The vector $X(t)$ gives the spatial location with respect to Wind of a point moving with the magnetic flux line, which at time t_0 went by GEOTAIL; hence its mathematical expression is

$$X(t) = r_{WI}(t) - r(t),$$

with $r(t) = r_{GE}(t) + <u_{dr}> \Delta t$.

In this way, $X(t)$ takes into account the effect of the drift of the IMF field line (see Figure 2). ($X(t)$ points toward Wind.) We define the closest approach condition as
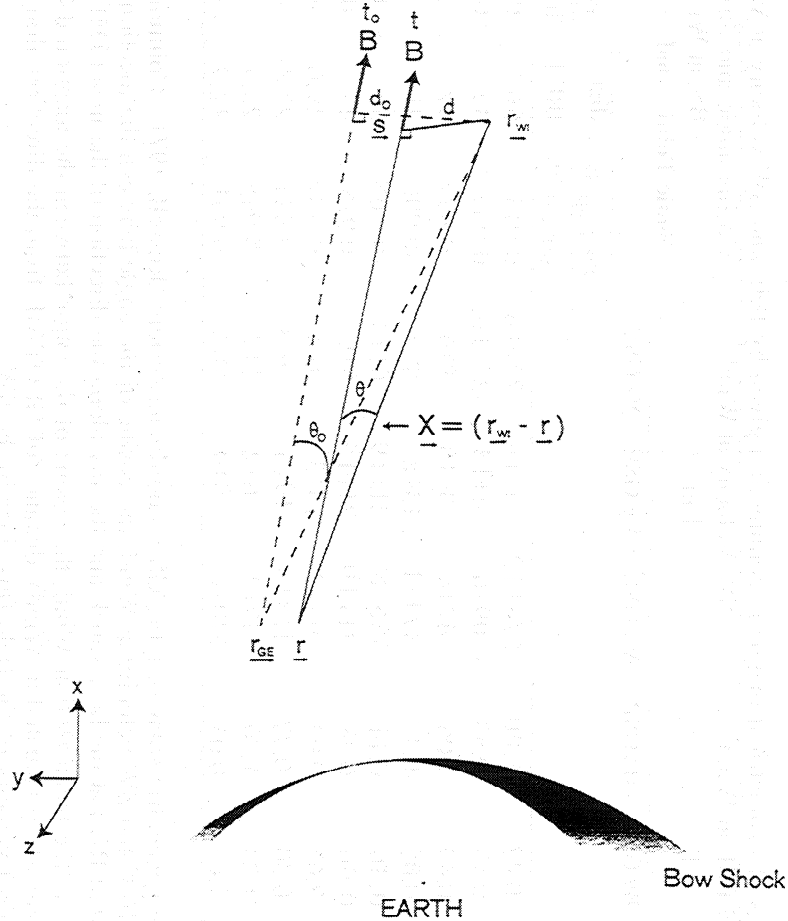

Figure 2. Schematic representation of the condition of closest approach of a flux line, which moved at t_0 by GEOTAIL and became closest to Wind at t, in a geometry typical to events 1 to 9 presented in Table 1. Here r_{GE} is the vector location of GEOTAIL in the SW in the near upstream region of the Earth's bow shock. The solid line labeled on the top with the letters B and t is along the mean direction of the magnetic field flux line (i.e., $<B>$) at time t of its closest approach. This flux line went by r_{GE} at time t_0 (dashed line). The parameter r_{WI} is the vector location of Wind far upstream from the Earth's bow shock; $r_{WI} - r_{GE}$ is the value of X at time t_0 (i.e. $X(t_0)$) and $d_0 = |X(t_0)| \cos(\theta_0)$ is the corresponding distance from Wind to the location of the field line through r_{GE}. The distance from Wind to its closest approach to the mean magnetic field B, at the vector location s and time t, is $d = |X| \cos(\theta)$, with $X = r_{WI} - r$.

$$\frac{d}{dt} \langle B\rangle/\langle B\rangle \cdot X(t)/|X(t)| = 0. \tag{1}$$

We determine the angle θ between $\langle B\rangle$ and $X(t)$ ($\theta = \arccos[\langle B\rangle/\langle B\rangle \cdot X(t)/|X(t)|]$) corresponding to the closest approach. The evaluation simplifies with $X(t) = DX - \langle u_{dr}\rangle \Delta t$, and an approximately constant value $DX = \langle r_{WI}(t_0)\rangle - \langle r_{GE}(t_0)\rangle$, after dropping the slow variation in location of the spacecraft.

Therefore, the derivative in (1) simplifies to
$$\frac{d}{dt} X(t)/|X(t)| = -\langle u_{dr}\rangle/|X(t)| + X(t) (X(t) \cdot \langle u_{dr}\rangle)/|X(t)|^3$$
because $\langle B\rangle/\langle B\rangle$ is assumed to be constant, and then by taking the scalar product with $\langle B\rangle/\langle B\rangle$, we can write the solution to (1) as

$$\langle B\rangle/\langle B\rangle \cdot [\langle u_{dr}\rangle |X(t)|^2 - X(t) (X(t)\cdot\langle u_{dr}\rangle)] / |X(t)|^3 = 0, \tag{2}$$

which has two solutions. The first solution is

$$X(t) \cdot \langle u_{dr}\rangle = 0 \tag{3}$$

because by definition $\langle u_{dr}\rangle \cdot \langle B\rangle = 0$, which implies that at closest approach $\langle u_{dr}\rangle$ is orthogonal both to $\langle B\rangle$ and $X(t)$, i.e. for the smallest $\theta(t)$. This occurs in a difference in time Δt.

The second solution is

$$\langle u_{dr}\rangle |X(t)|^2 - X(t) [X(t) \cdot \langle u_{dr}\rangle] = 0, \tag{4}$$

which reduces to the condition $(\langle u_{dr}\rangle \cdot DX)^2 = \langle u_{dr}\rangle^2 (DX)^2$ if we use $X(t) = DX - \langle u_{dr}\rangle \Delta t$. This can be solved only if $\langle u_{dr}\rangle // DX$ since $\langle u_{dr}\rangle \perp \langle B\rangle$, and this would imply $\langle B\rangle \perp DX$ (see equation (1)), which corresponds to no minima and does not fit into the present cases where $\langle B\rangle$ is oblique to DX.

From the first solution, substituting $X(t) = DX - \langle u_{dr}\rangle \Delta t$ in (3), we obtain not only

$$\Delta t = DX \cdot \langle u_{dr}\rangle / |\langle u_{dr}\rangle|^2, \tag{5}$$

but also $X(t)$ and $\theta(t)$. Our analysis identifies $\cos(\theta(t))$, $\theta(t)$, and the distance

$$d(t) = \sin[\theta(t)] |X(t)| \tag{6}$$

as indicative of the approximate magnetic conjunction condition, measured from the closest location $\langle s(t)\rangle$ to Wind (represented in Figure 2 by $\underline{S}$). $\langle s(t)\rangle$ marks the closest approach to Wind of the ray along $\langle B\rangle$ (IMF direction measured at Wind) which at t_0 went through the GEOTAIL location ($\langle r_{GE}(t_0)\rangle$) (see Figure 2). Table 3 presents Δt, $\cos[\theta(t)]$, $\theta(t)$, and $d(t)$, which are solutions to the investigated magnetic conjunction condition. In addition, Table 3 illustrates the difference of the mean IMF and plasma moments (H^+) for the events from Table 1 observed between Wind and GEOTAIL.

The assumptions involved in the above derivation are similar to those used by *Greenstadt and Baum*, [1986], in their definition of the foreshock's V-B plane and determination of an unambiguous boundary for the ion foreshock whenever the angle between the IMF and the SW flow is $\sim 30°$ or larger [see also *Le and Russell* [1992].

In most cases we expect the resulting mean minima $d(t)$ to be valid within one or two RE. Remember that the analysis above neglected the bending of the IMF guiding centers close to the bow shock, near GEOTAIL (see Table 3), and its extension in the IMF toward the upstreaming region. This effect has been observed [see, e.g., *Kelly et al.*, 1986, Figure 2, panel 4]. No magnetic conjunction occurred for event 10. In this case the large difference for the IMF (bottom row in Table 3) is a consequence of observations of the ion foreshock from regions located in IMF domains of opposite polarity.

Tables 2 and 3 show the anticorrelation between the value of Δt and the magnitude of the drift velocity of the IMF lines. A larger Δt may also result from a longer distance in the displacement of the mean orientation of the $\langle B\rangle$ flux lines, from GEOTAIL to the closest approach to Wind. This interpretation is consistent with earlier statistical studies [*Kelly et al.*, 1986; *Russell et al.*, 1980].

4. Far and Near Ion Foreshock: One Example (June 11, 1995)

Typical characteristics of the wave and particle activity during these magnetic conjunction events are illustrated with the June 11, 1995 event, i.e. event 4 in Table 1. Nevertheless, this is atypical in two key aspects. First, the drift velocity of the B field lines was extremely slow (Table 2). Second, during a subinterval the conditions for a sequential bow shock-GEOTAIL-Wind magnetic conjunction are satisfied (see section 5). From Table 2 we extract the following general information for the event. The mean direction of the IMF deviates less than 2° from the imaginary line connecting the Sun and the Earth, and its magnitude was 4.26 nT. The mean velocity of the SW deviates approximately 2° 20' from a radial direction from the Sun, and its magnitude is 374.3 kms^{-1}. A line along the mean IMF at Wind is within 20 RE of the location of the bow shock's sonic point and 32 RE of GEOTAIL, and the convection velocity at Wind is almost stagnant.

In Figure 3 we present the time profiles for 1 day of the 1-min. averaged IMF and other SW parameters measured by Wind located at ~ 230 RE. Figure 3a shows that the ram pressure of the SW varies between 1.2 and 0.8 nPa, which is less than half of the average value. As seen from Figure 3b, the intensity of the IMF appears to change smoothly between ~ 6 and 4 nT, between 0300 and 2100 UT. Figures 3c and 3d show that during this interval the direction of the IMF with an orientation dawn-dusk lies approximately in the plane of the ecliptic which gradually becomes radial from the Sun, and remains so, between 1230 and 2100 UT. As seen from Figures 3e-3g, the SW has an approximately steady velocity ranging from 400 to 350 km s^{-1}. During this interval the plasma density is also steady, ranging from 4 to 6 particles per cm^3 (see Figure 3h). Thus the SW conditions are very quiet on June 4, 1995. This is indicative of a period without any convected structure, with the possible exception of a buildup in the plasma temperature (see Figure 3i), as seen for example between 0830 and 1530 UT. During this event, GEOTAIL was located in the ion foreshock almost all the time (at about 14 RE from the bow shock), as indicated by the nearly continuous presence of energetic ions from ~ 1330 to 2130 UT.

In Figure 4 we present energetic ion fluxes averages and 3-s averages of IMF measured by GEOTAIL from 1330 to 2130 UT. Figure 4a gives the energetic ion data (flux intensities averaged over all azimuthal directions and integrated along the polar direction) for channels 61.5 to 73.7 keV, and 89.3 to 110.0 keV. The energetic ion flux fluctuations are also observable in the high-resolution data (6-s data, 61.5 to 73.7 keV channel).

Table 3. Solution to Equation 3 of the magnetic conjuction condition between Wind and GEOTAIL and the difference in the IMF and SW conditions at Wind and GEOTAIL.

| Event | Parameters to the Magnetic Conjunction | | | | Average Value Differences | | | | | | |
| | Δt, min. | $\cos(\theta)$ | θ, deg. | d RE | $\Delta B = (B_{GE} - B_{WI})$, nT | | | $\Delta V = (V_{GE} - V_{WI})$, kms^{-1} | | | ΔNp, cm^{-3} |
					$\Delta B[x]_{GSE}$	$\Delta B[y]_{GSE}$	$\Delta B[z]_{GSE}$	$\Delta V[x]_{GSE}$	$\Delta V[y]_{GSE}$	$\Delta V[z]_{GSE}$	$N_{GE}-N_{WI}$
1	-30.4	0.997	4.51	18.3	-0.7±0.1	-0.07±0.07	0.8±0.1	40±40	-20±40	16±40	-0.2±1.0
2	-29.7	0.997	4.54	17.2	-0.8±0.1	0.3±0.1	0.23±0.05	13±13	-26±20	11±25	0.6±1.2
3	-41.9	0.9997	178.65	5.5	0.8±0.2	0.1±0.2	0.2±0.2	22±26	0±40	-5±20	-0.7±1.6
4	-400.4	0.9989	177.3	9.8	0.06±0.06	-0.70±0.07	0.4±0.1	22±3	-7±10	-11±13	-0.5±1.7
5	-76.2	-0.995	174.29	19.0	0.6±0.2	-0.4±0.2	0.5±0.4	30±20	-50±30	-20±20	-0.1±0.8
6	-47.7	0.9945	6.0	18.0	-0.4±0.7	0.2±0.7	-0.2±0.2	21±40	-27±35	-10±20	-0.8±1.5
7	-28.7	0.9986	177.0	7.3	0.8±0.1	-1.9±0.1	-0.9±0.1	8±9	16±10	-3±7	0.7±3
8	-14.3	0.9784	168.07	10.1	0.30±1.8	-0.4±2.4	0 ±2	8±8	-30±12	-8±9	-1.7±2.0
9	-7.25	-0.956	162.91	19.6	0.07±0.06	-0.15±0.07	-1.36±0.06	16±13	8±18	-10±13	-7±4
10	***	***	***	***	-5.0±0.1	-2.1±0.1	0.4±0.1	26±7	-25±20	-35±13	0.7±0.6

Event number (column 1), Δt delay for the closest approach to Wind of the flux line passing at t_0 by GEOTAIL (column 2), the cosine of the angle $\theta(\Delta t)$ (defined in equation 1; see Figure 8) corresponding to the closest approach to magnetic conjunction between Wind and GEOTAIL (column 3), the value of $\theta(\Delta t)$ (column 4), the distansce $d(\Delta t)$ of Wind to magnetic conjunction (column 5), the difference in the mean value of the IMF and SW parameters at Wind and GEOTAIL (columns 6-12).
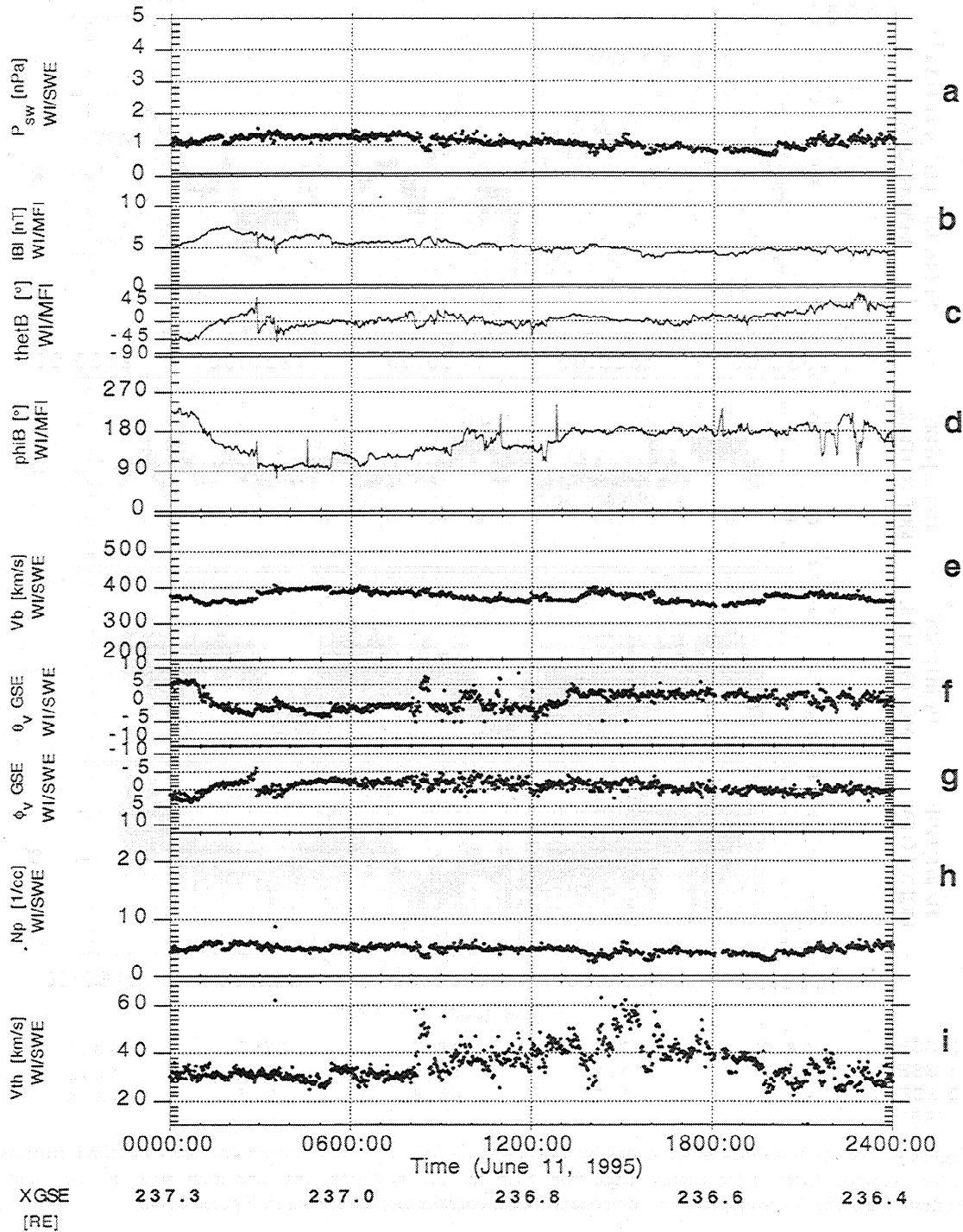
Figure 3. The time profiles of the IMF and SW plasma parameters at Wind (~1-min averages) on June 11, 1995: (a) the ram Pressure $m_p V_x^2$, (b) the magnitude of the IMF, (c) the latitude angle θ_B of the IMF, (d) the azimuth angle ϕ_B of the IMF, (e) the SW speed (protons), (f) the latitude angle θ_V of the SW speed, (g) the azimuth angle ϕ_V of the SW speed, (h) the SW proton density Np, and (i) thermal speed V_{th}

Figures 4b-4d show that the fluctuations in the IMF appear to coincide with the energetic ion flux enhancements seen in Figure 4a. These Figures 4a-4d show that the enhanced magnetic field fluctuations with larger amplitude correspond to direction(s) perpendicular to the IMF mean field <**B**>, which is pointing approximately in the x-GSE direction.

In Figure 5 we present the energetic ion data at GEOTAIL. In Figures 5c and 5b, we present the energetic ion fluxes versus

the azimuth for two intervals of interest from 1500 to 1520 UT and from 1530 to 1551 UT. This representation of the data depicts the clear nature of the energetic ion population (63-71 and 89.3-110.2 keV channels), which shows the comparable fluxes in all directions, i.e., from parallel to transverse with respect to mean IMF. This is a good signature of the scattered energetic ion population. Figures 5c and 5d present the energetic ion fluxes (63-71, 89.3-110.2, and 137-173 keV
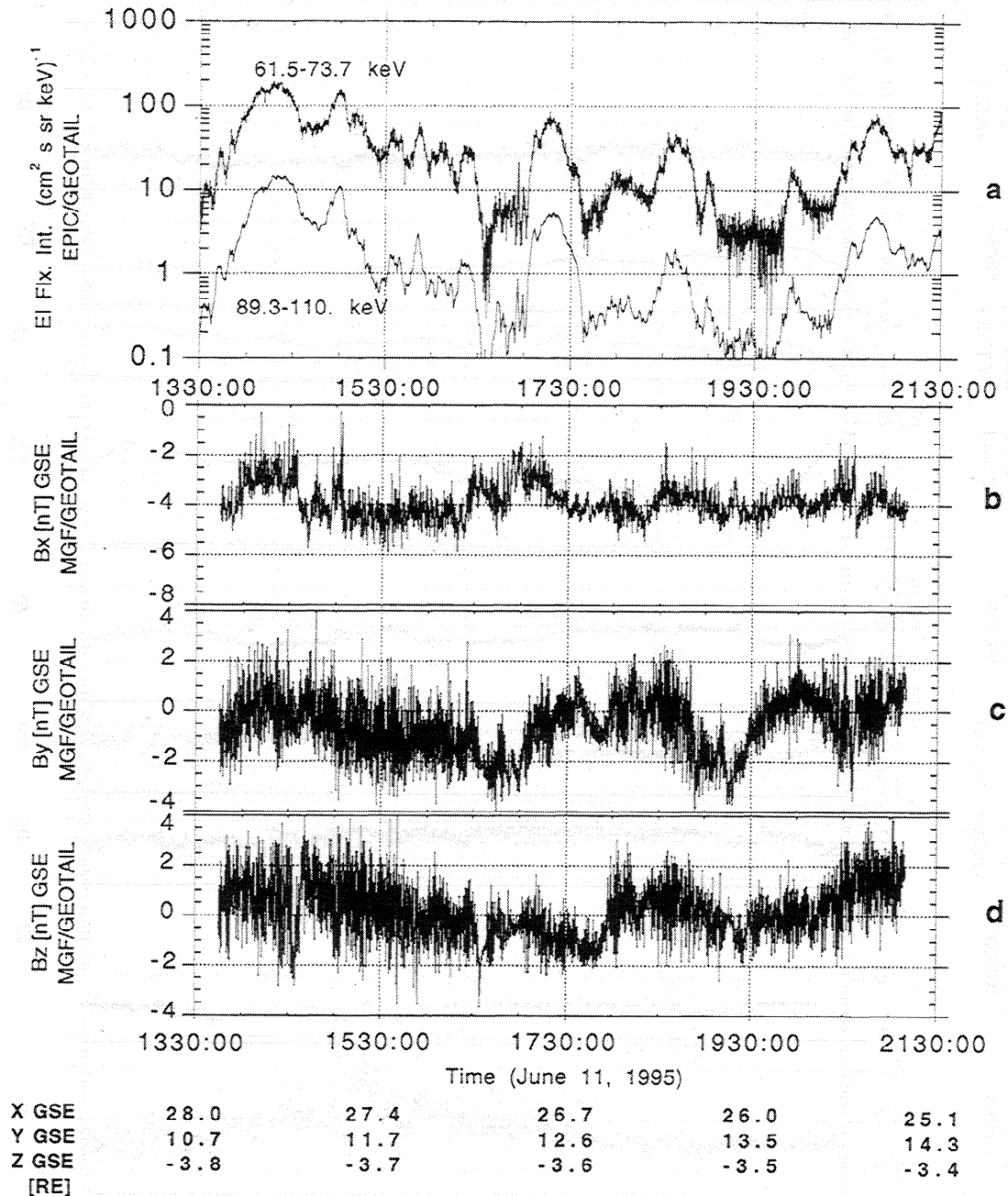
Figure 4. The ion foreshock observations by GEOTAIL on June 11, 1995. Figure 4a shows the time profiles of the averaged fluxes in the energy range from 61.5 to 73.7 keV (top line) and from 89.3 to 110.7 keV (bottom line). The 3-s averaged IMF components (GSE coordinates) are shown in Figures 4b-4d.

channels) as time series between 1430 and 1600 UT. Figure 5c shows the energetic ion fluxes in the upstream direction approximately along the IMF; and Figure 5d shows the energetic ion fluxes in the dawn direction, i.e., normal to the IMF. During these intervals, enhancements in magnetic field fluctuations (see Figure 4), as well as in the energetic ion fluxes (Figures 4 and 5), were observed. The energetic ion data show an approximately exponential differential flux spectrum $df(E_{EI})/d\Omega \propto \exp[-(0.08\pm1)E_{EI}]$, in energy ($E_{EI}$), which is a good signature of the scattered energetic ion population [Ipavich et al., 1979; Eichler, 1981]. These nearly diffuse energetic ion populations show strong fluctuations in the 6- and 48-s average fluxes, as seen in Figures 5c and 5d.

For the same event we present the 3-s averaged IMF and 12-s averaged energetic ions measured at Wind from 1500 to 1630 UT in Figure 6. Magnetic fluctuations (ULF waves) are present from 1500 to 1530 UT (Figure 6a), which are much weaker in comparison with those observed at GEOTAIL (Figure 4). During the interval the energetic ions (40-140 keV) appear to be at the background level (bottom panels, Figure 6b and 6c). The mean IMF at Wind appears either disconnected or connecting to the far tailward region of the bow shock in the nightside. Figure 7 presents the approximate relative location of Wind and GEOTAIL with respect to the Earth's bow shock, in the Z-X(GSE) and Y-X(GSE) coordinate system, during this time interval. The directions of the IMF, as seen from Figure 7,
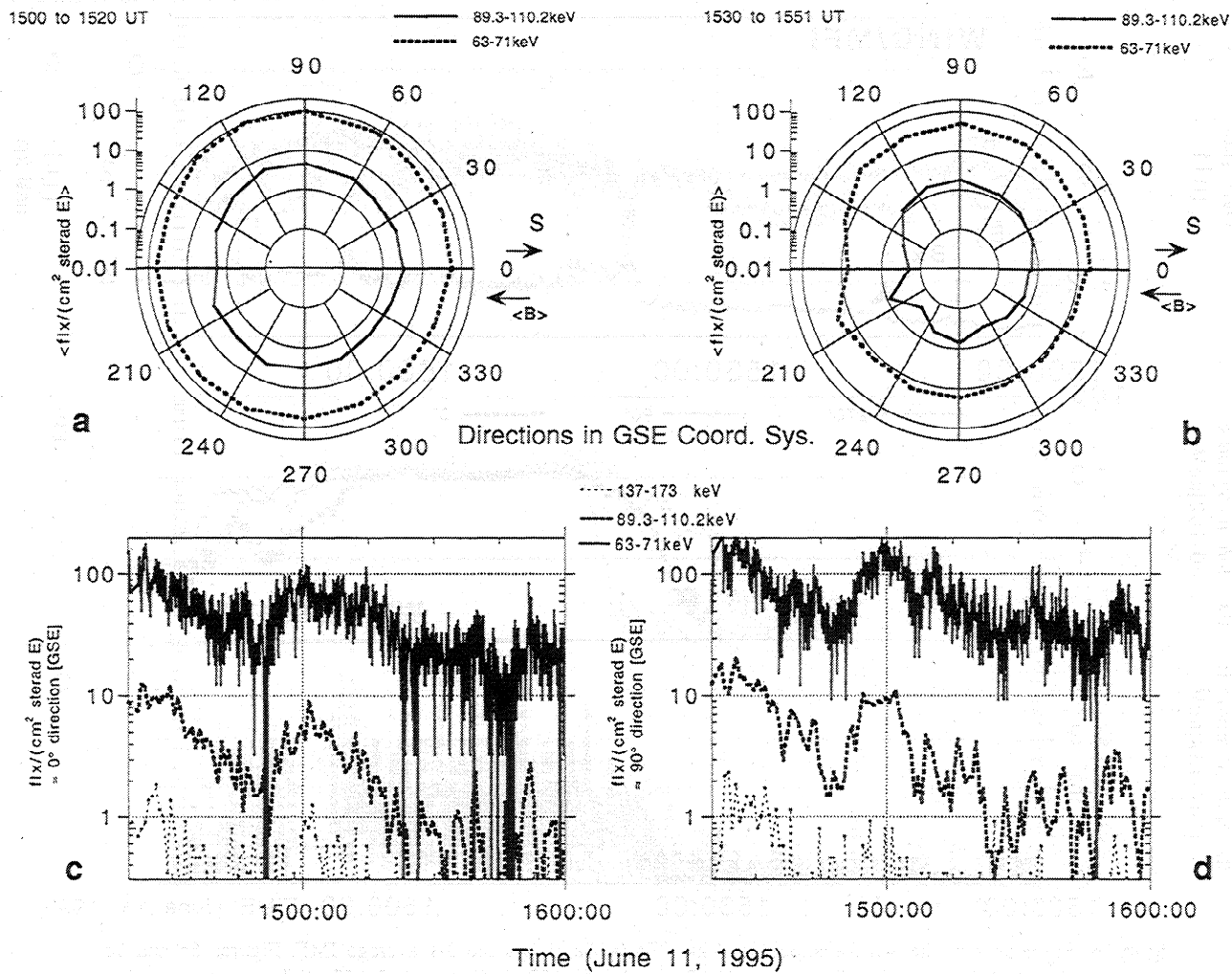
Figure 5. EPIC/GEOTAIL energetic ion (EI) observations on June 11, 1995. Figures 5a and 5b display the flux of the EI corresponding to channels 63-71 and 89.3-110.2 keV, in polar coordinates, for two time intervals given in the top right corners. The arrow labeled "S" on the right side of Figures 5a and 5b indicates the sunward direction. The direction of the second arrow (<B>) gives the approximate orientation of the mean IMF. Figures 5c and 5d show the time profiles of the fluctuating fluxes 63-71 keV (6-s averages) and 89.3-110.7 and 137-173 keV (48-s averages) directed sunward and duskward, respectively (GSE coordinate system).

indicate that the mean IMF is connected to the bow shock in the dayside from 1530 to 1600 UT. In fact, during this interval the enhanced oscillations in the IMF and the energetic ion fluxes are observed (Figure 6). The ion fluxes are more intense in the lower energetic channels. This (approximately) exponential energy partition indicates the scattered nature of the upstreaming energetic ion population at Wind. Both 40-100 keV and 100-140 keV ion fluxes show comparable intensities in the directions 0°, 90°, and 270° (GSE coordinate system), in a plane containing the direction of the mean IMF ($\phi_B \cong 180°$, $\theta_B \cong 0°$ at Wind). This pitch-angle analysis presented in Figure 6 illustrates the strong similarities of the energetic ions at Wind far from the bow shock and the energetic ions at GEOTAIL very close to the bow shock (see Figures 5a-5d).

A transformation of the IMF data to frequency space, for the time interval from 1500 to 1600 UT, allows the ordering of the wave excitations with respect to the proton cyclotron frequency ($f_{cp} \cong 0.065$ Hz). Figure 8 presents the IMF frequency spectra at GEOTAIL (Figure 8a) as well as at Wind (Figure 8b).

The power spectrum for each component of the IMF is shifted by one decade, in order to separate them from each other in the low-frequency part of the spectral plot. These spectra show that the observed excitations have a clear upper cut off frequency near f_{cp}, suggesting that these magnetic field fluctuations are either blue-shifted hydromagnetic modes, or red-shifted cyclotron waves in the SC frame of reference. A careful examination of Figure 8 further reveals that the Fourier-analyzed magnetic field data shows a well-developed broad-banded plateau in the power spectrum of these transverse modes near the bow shock (GEOTAIL), in comparison with that of far upstream as observed by Wind. This difference arises mostly because this interval covers the times of both good and bad connection of Wind to the dayside ion bow shock. We also notice that the power of the transverse wave fluctuations (~ y-GSE, and z-GSE) is about 20 times larger than that of the parallel fluctuations (~ x-GSE) in the far, as well as near, ion foreshock regions in the frequency range $1/10 < f/f_{cp} < 2/3$.

In Figure 9 we present the frequency power spectra, at GEOTAIL and Wind, of the IMF and energetic ions for
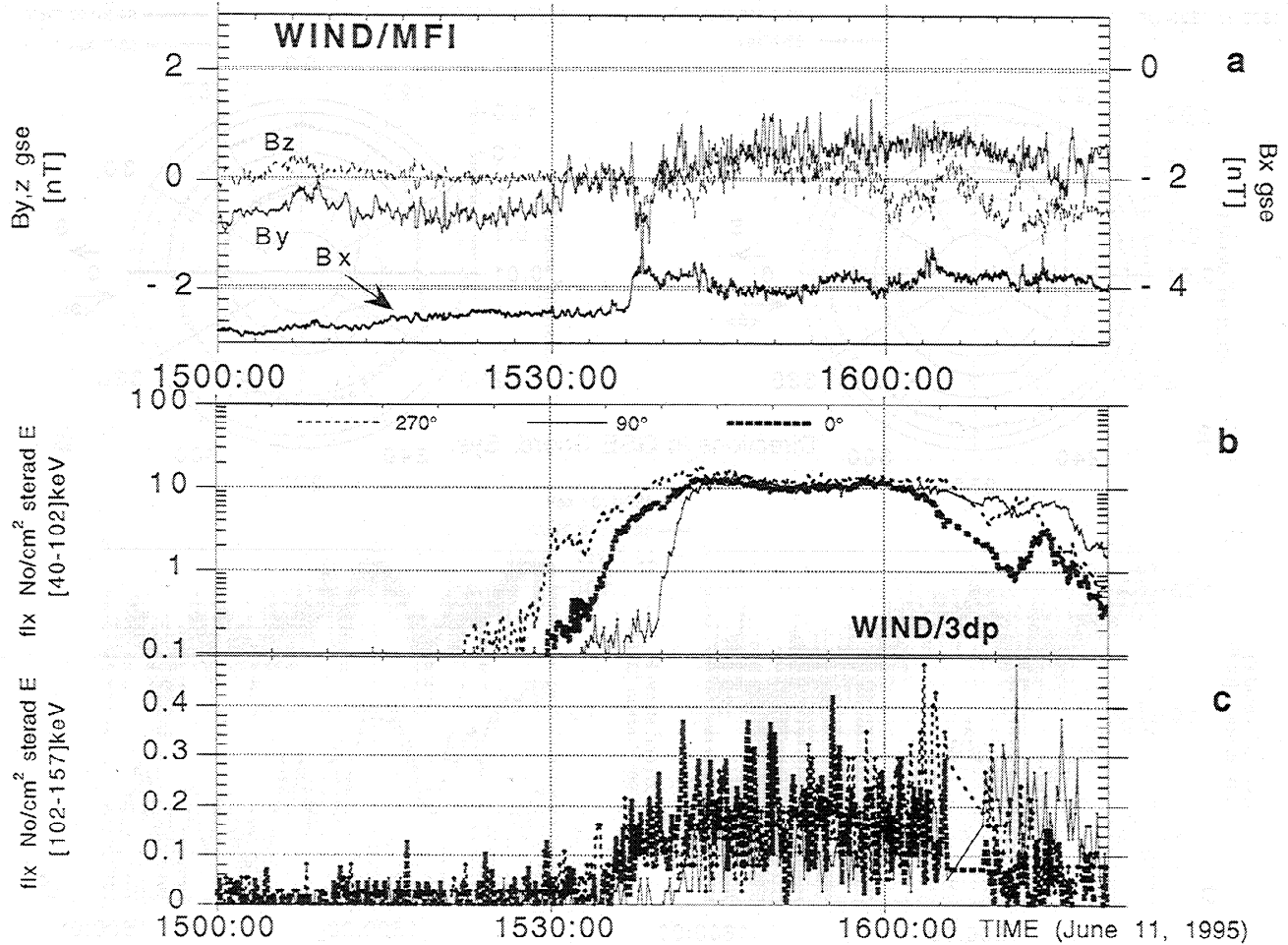
Figure 6. Signatures of the ion foreshock at Wind. Figure 6a shows the 3-s average IMF. Figures 6b and 6c show the time profiles of the fluctuating EI fluxes in 40-102 keV and 102-157 keV energy ranges, respectively. In these two plots the fluxes correspond to the three pitch angles 270°, 0°, and 90° (approximately the dawnward (- y_{GSE}), sunward (x_{GSE}), and duskward (y_{GSE}) directions, event 4, June 11, 1995).

overlapping times when both SC were well connected to the dayside bow shock region. The energetic spectrum of upstream ions observed by Wind is very similar in its exponential shape to the one observed by GEOTAIL, suggesting that they are probably of a common origin. This similarity persists even for the fluctuations of the energetic ion fluxes, as well as the ULF waves as shown in Figure 9. Figure 9a shows the total power spectrum of the magnetic field fluctuations, both near and far, from the bow shock for overlapping time intervals when Wind is well in the (far) ion foreshock region. Figure 9a shows that the power spectra plateaus of excited ULF waves (~ 0.008 to 0.06 Hz) are similar in the close as well as the far ion foreshock regions. Figure 9b shows the added power spectra of the energetic-ion flux fluctuations at 0°, 180°, and 270° pitch angles, both far and close to the bow shock. These energetic ion and ULF power spectra appear to be alike in the development of a plateau for the same frequency range. These power spectra of the energetic ion fluctuations correspond to the fluxes of 61.5-89.3 keV ions at GEOTAIL, and from 40-102 keV ions at Wind. These fluxes cover different energy ranges and the total power of their fluctuations is much higher than that of magnetic field fluctuations. (Notice that for presentation purposes the strength of the power spectrum observed by Wind has been multiplied by a factor of 10.)

5. Interpretation and Testing of Magnetic Conjunction Conditions

We proceed next to test the quantitative evaluation of the magnetic conjunction condition for event 4 in Table 3. First we notice that all cases in Table 3 have a negative Δt, indicating that the flux lines passing by GEOTAIL approached Wind first, i.e., the mean direction <B> moves away with time from its closest approach to a magnetic conjunction between both spacecraft. A first implication of this result is that in general there is no sequential (causal) magnetic conjunction between the bow shock, GEOTAIL, and Wind regions. A second implication is that Wind is closer to the foreshock boundary, given the respective distances of the spacecraft Wind and GEOTAIL to the bow shock. This can easily be understood from the analysis by *Le and Russell* [1992], when applied to a typical spacecraft configuration of our study, as shown in Figure 2 [see also *Bonifazi and Moreno*, 1981]. These interpretations may not hold in a closer analysis, however, as demonstrated in the following example.

It is clear from Tables 2 and 3 that the case least affected by the drift velocity is event 4 of June 11, 1995. For example, from 1500 to 1600 UT the mean drift velocity <u_{dr}> is extremely small, and the mean <B> responsible for such a
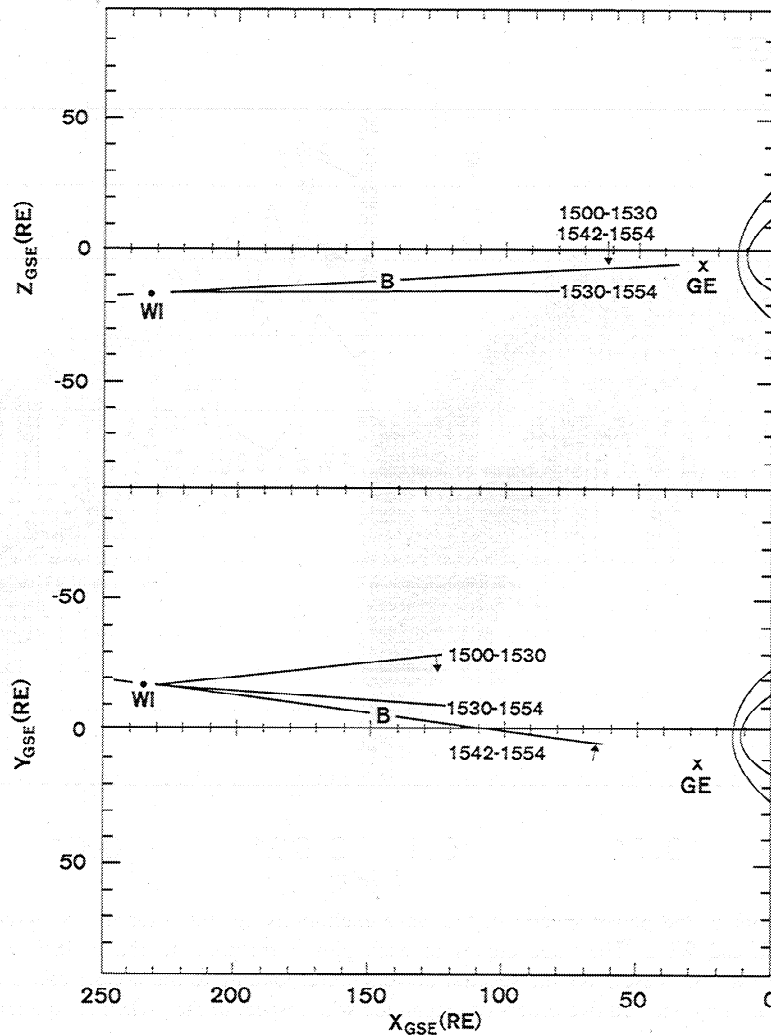
Figure 7. The spatial coordinates of Wind (WI) and GEOTAIL (GE) (GSE coordinate system) with respect to the orientation of the mean IMF <B> represented as solid lines for three selected time intervals (given in the Figure 7) on June 11, 1995. Also shown are the nominal locations of the Earth's bow shock and magnetopause. Arrows on the magnetic field lines (at the bottom of Figure 7) give the drift direction $<u_{dr}>/|<u_{dr}>|$ of the IMF.

negligible drift arises as a result of the cancellation of changes in the <By> and <Bz> components, which are significant.

First, from 1500 to 1530 UT the mean IMF value at Wind is <B_{WI}> = (-4.67, -0.57, 0.10). This indicates that slowly drifting flux lines exist at GEOTAIL, and a solution for their closest approach to Wind can be written $\theta(\Delta t=-100 min)= 174°40'$, and $d(\Delta t)= 19$ RE. From here on we assume $t_0 = 0$ and hence the minimum-distance time $\Delta t = t$. The negative value of Δt implies that the IMF flux line drifts close to Wind first and about 100 min later to the location of GEOTAIL. In section 4 we have shown the existence of intense particle and wave enhancements at GEOTAIL during this interval. The orientation of <B_{WI}> suggests that at this time the IMF flux lines came very close to Wind, but they were either not connected to the bow shock (see Figure 7) or connected to the bow shock on the far nightside west of r_{sp} and r_{GE}. Nevertheless, low-amplitude ULF waves up to f_{cp}, which are predominantly transverse with respect to <B_{WI}> (see Figure 6), are observed at Wind.

Second, from 1530 to 1554 UT, with <B_{WI}> = (-4.11, 0.23, 0.09) the solution for closest magnetic conjunction is

obtained as $\theta(\Delta t=8.2min) = 174°50'$, and $d(\Delta t)= 18.99$ RE. The positive sign in Δt implies that the flux lines drift first to GEOTAIL and ~ 8 min later they are within about 19 RE of Wind. This is consistent with the geometric orientation of <B_{WI}>. The orientation of <B_{WI}> during this interval also indicates that the IMF flux lines at Wind are connected geometrically to the dayside of the bow shock. This is further supported by the observation of (1) the scattered energetic ion fluxes (40-140 keV) being above background level and (2) the simultaneous enhancements in the amplitudes of the transverse ULF wave oscillations at Wind (Figure 6). In particular, from 1542 to 1554 UT, when <B_{WI}> = (-4.03_5, 0.50_5, 0.22) the conditions for the sequential magnetic-conjunction bow shock-GEOTAIL-Wind are given, with the solution of a time delay $\Delta t= 5.1$-min, i.e. positive, $\theta(\Delta t=5.1-min)=179°20'$, and the very small $d(\Delta t)= 2.6$ RE. These solutions of equation (3) satisfy the ion foreshock conditions observed at GEOTAIL and Wind for event 4.

A more common situation is illustrated by event 8 (August 25, 1995), during which large traveling convective structures
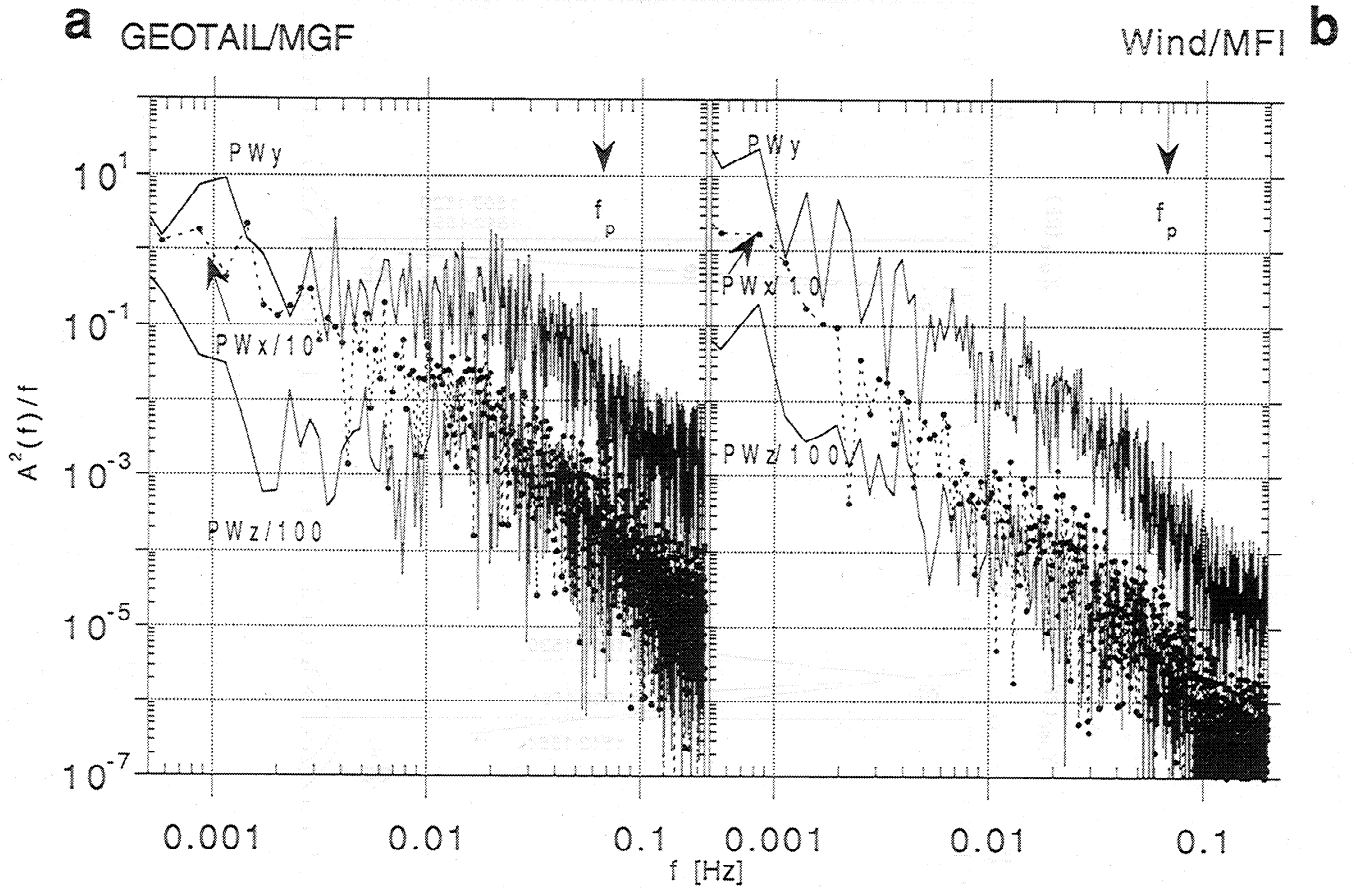
Figure 8. The plots of the power spectra of the wave excitations for the interval 1500-1600 UT, June 11, 1995, at GEOTAIL and Wind. The three curves in each plot correspond to the x-GSE, y-GSE, and z-GSE components of the IMF. In these plots the spectral powers corresponding to the x-GSE and Z-GSE components of the IMF are reduced by one and two orders of magnitude with respect to the y-GSE component.

with large-amplitude variations in the IMF (ΔBs) are observed. For this event, enhanced energetic ions and ULF waves are observed at Wind from 1627 to 1633 UT. During this subinterval (at Wind, <B> = (-4.66, 2.12, -1.06)), the magnetic conjunction bow shock-Wind-GEOTAIL is not achieved since Δt was negative. However, the values of $\theta(t)$ and $d(t)$ indicate that the energetic ions are likely to be associated with the same source region in the bow shock (closest $\theta(\Delta t = -8.2$ min$) = 174°51'$, $d(\Delta t) = 6.78$ RE). This was an event for which a change in the sign of the IMF GSE-z component to positive 0.5 nT would have put the two spacecraft on exact magnetic conjunction for a positive Δt.

6. ULF Wave Excitations During the Scattered Energetic Ion Intervals

Some plasma characteristics relevant to our analysis of ULF waves are presented in Table 4. They include the proton cyclotron frequency $f_{cp} = (e/m_p)$ ($B/2\pi$), the Alvén speed $V_A = |B|/\sqrt{(4\pi N_p)}$, the electron and proton temperatures, the sound speed $V_S = \sqrt{(5/3)(k/mp)(T_e + T_i)}$, and the Mach numbers. The proton cyclotron frequency f_{cp} varies from 0.04 to 0.12 Hz, and the Alfvén speed V_A varies from 20 to 60 km s^{-1}. The maxima-estimated Alfvèn and sonic Mach numbers M_A and M_S (calculated at the bow shock sonic point) are estimated to lie in the ranges from 6 to 15, and 5 to 9, respectively.

In the near upstream regions the f_{cp} is lower than those corresponding to far upstream regions (except in event 4 when they are equal), meaning that the magnitude of the mean IMF is larger farther upstream than closer to the bow shock. There are no equivalent correlations for the Mach numbers in the near and far ion foreshock regions because the Mach numbers depend not only on the IMF, but also on other SW plasma parameters.

For the separation of the IMF fluctuations into transverse and compressional modes we use the analysis technique given by *Sonnerup and Cahill* [1967] [see also *Harvey et al.* 1981]. First, we transform the GSE coordinate system into the coordinate system with the x axis along the mean IMF <B>. We then perform a direct analysis by evaluating the 1-min averages given by

$$\overline{B} = \frac{1}{N} \sum_i^N B_i \qquad (7)$$

of the 3-s average IMF, i.e. for N = 20. In this minimum variation analysis we perform a rotation to the orthogonal system (Xc, Yc, Zc) with the direction Xc along $\overline{B}/|\overline{B}|$. In this manner we obtain the field fluctuations

$$\delta By = By_c$$
$$\delta Bz = Bz_c \qquad (8)$$
$$\delta Bx = (Bx_c - \overline{B})$$

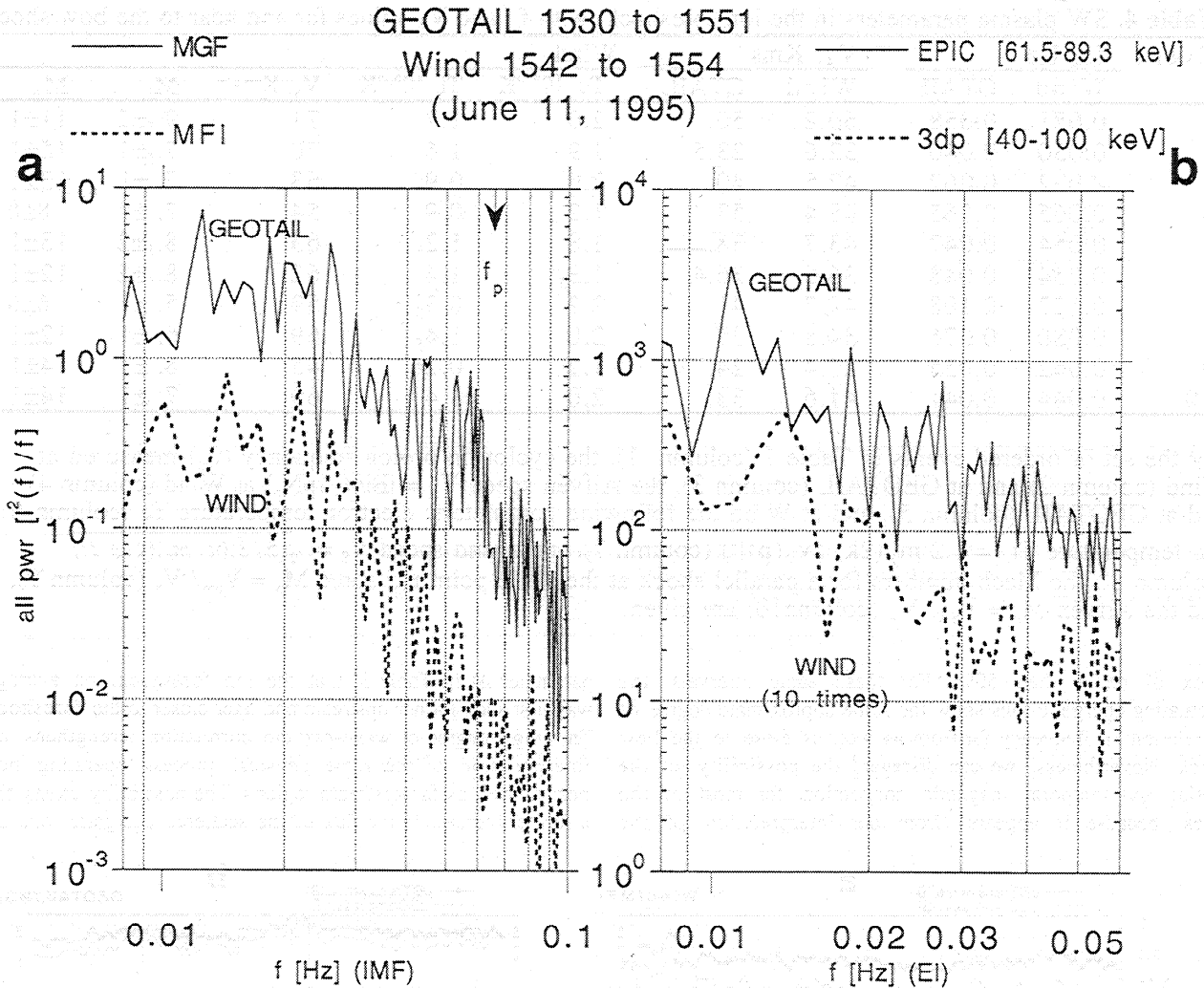and check the adequacy of the time interval selected and the

Figure 9. Figure 9a shows the total power spectrum of the ULF wave excitations at GEOTAIL and Wind for selected intervals. Figure 9b shows the corresponding power spectrum of the fluctuating energetic ion (EI) fluxes at GEOTAIL and Wind. Here the spectral powers corresponding to the EI fluxes at Wind are increased by one order of magnitude for a better representation.

quality of the transformation by testing that the conditions δ Bx $\ll$ δ By, δ Bz were well satisfied (like in Figures 4 and 6, a case when Xc ~ X(GSE)). Next, we evaluate (using the 3-s averages of Bx_c, By_c, and Bz_c) the compressional

$$\delta B_c^2 = (|B|^2 - \bar{B}^2) \qquad (9)$$

and the transversal

$$\delta B_T^2 = \text{trace} \left(\overline{B_\alpha B_\beta} - \bar{B}_\alpha \bar{B}_\beta \right) \qquad (10)$$

fluctuations, with α, β = x, y, z, for each 1-min window [*Harvey et al.*, 1981]. This separation allows a direct comparison of the relative strength of the transverse modes with respect to compressional ones (see Figure 10). The present observations indicate that the mHz transverse modes dominate the compressional waves, by a ratio of 7 or larger, in the far upstream regions. Transverse modes are dominant near the bow shock by a smaller ratio (~ 3 in most cases). These transverse ULF waves appear to be broadbanded and strong when they are coincident with the enhanced bursts of strongly scattered energetic ion fluxes present far (Wind) and close (GEOTAIL) to the bow shock (Figure 8).

For each event at Wind and GEOTAIL, Table 5 presents the mean transversal and compressional fluctuations of the IMF relative to the mean field <|B|>, and the first two moments of the power spectrum of the total ULF excitations. The ULF wave power peaks in the frequency range ~ 1/10–2/3 f_{cp} (see Table 5) and coincided with the observed fluctuations in the ion fluxes which also have a broadbanded spectrum in the same frequency range (Figure 9). (For each event the power of the excitations listed in Table 5 is obtained by evaluating its value and then subtracting the measured value for the spectrum found to have the lowest power, corresponding to the time interval 1348 to 1448 UT, on June 11, 1995, at Wind.) The broad nature of the ULF centroid seems to favor the possible presence of strongly turbulent ULF wave conditions (see, e.g., *Gary* 1981, and references therein]. It is interesting to note that for far and near ion foreshock conditions (in several of the presented events, for selected time periods) the shape of the power spectrum and its location in frequency, for the ULF waves, correlate well with fluctuations of the energetic ions. For some intervals there is a correlation far from as well as close to the bow shock in the position of most peaks and valleys in frequency space for the ULF fluctuations, with a correlation

Table 4. SW plasma parameters in the ion foreshock, with f_{cp} and V_A values far and near to the bow shock

Event	f_{cp}, Hz		V_A, Kms^{-1}		Wind				
	Wind	GTAIL	Wind	GTAIL	T_e, 10^5 °K	T_i, 10^5 °K	V_S, Kms^{-1}	M_S	M_A
1	0.071	0.058	60.2	50.	2.0	1.7	71	$9._5 \pm 2$	11 ± 1
2	0.050	0.040	32.6	23.5	1.9	1.6	70	$7._5 \pm 1$	15 ± 1
3	0.072	0.062	42.5	40.	2.0	0.9	63	$7. \pm 1$	13 ± 1
4	0.065	0.065	48.4	53.	1.2	0.9	54	$7. \pm 1$	8 ± 0.5
5	0.054	0.047	43.7	38.	1.8	1.2_5	65	$8._5 \pm 2$	13 ± 1
6	0.054	0.048	36.6_5	36.4	1.3_5	1.4	62	$8._5 \pm 2$	12 ± 1
7	0.127	0.108	49.7	41.	2.2	0.3_5	59	$5. \pm 1$	6 ± 0.5
8	0.080	0.076	34.8	37.	2.0	1.4_5	69	$6. \pm 1$	12 ± 1
9	0.062	0.055	20.4	24.	1.2	0.26	45	$8. \pm 1$	14 ± 1
10	0.044	0.041	41.6	33.	2.0	1.4	69	$7. \pm 1$	14 ± 1

For the set of ordered events in Table 1 (column 1), the cyclotron proton frequency (f_{cp}) measured at Wind (column 2) and at GEOTAIL (column 3), the Alfvén speed $V_A = |B|/\sqrt{(4pN_p)}$ at Wind (column 4) and at GEOTAIL (column 5), and at Wind the following parameters: electron temperature T_e (column 6), ion temperature T_i (= $1.2\ m_p/(2k)\ [V_{th}(p)]^2$) (column 7), the sound speed $V_S = \sqrt{(5/3)(k/m_p)(T_e + T_i)}$ (column 8), the Mach numbers for a parallel shock at the sonic point r_{sp}: sonic $M_S = V_{sw}/V_S$ (column 9), and the Alfvén $M_A = V_{sw}/V_A$ (column10) are given.

index of better than 50%. For these same intervals the fluctuating energetic ions show the same approximate degree of correlation in frequency far from as well as close to the bow shock. Nevertheless, we can disregard the possibility of the spatial and temporal magnetic connection for most of the cases, because it appears (from our interpretation of the parameter Δt in Table 3) that the ion foreshock, on average, was first seen farther upstream and later closer to the foreshock. This high degree of wave-particle correlation strengthens our interpretation of the same physical process operating both near as well as far upstream regions. The possibility exists that a further increase in the flux of the scattered energetic ions and
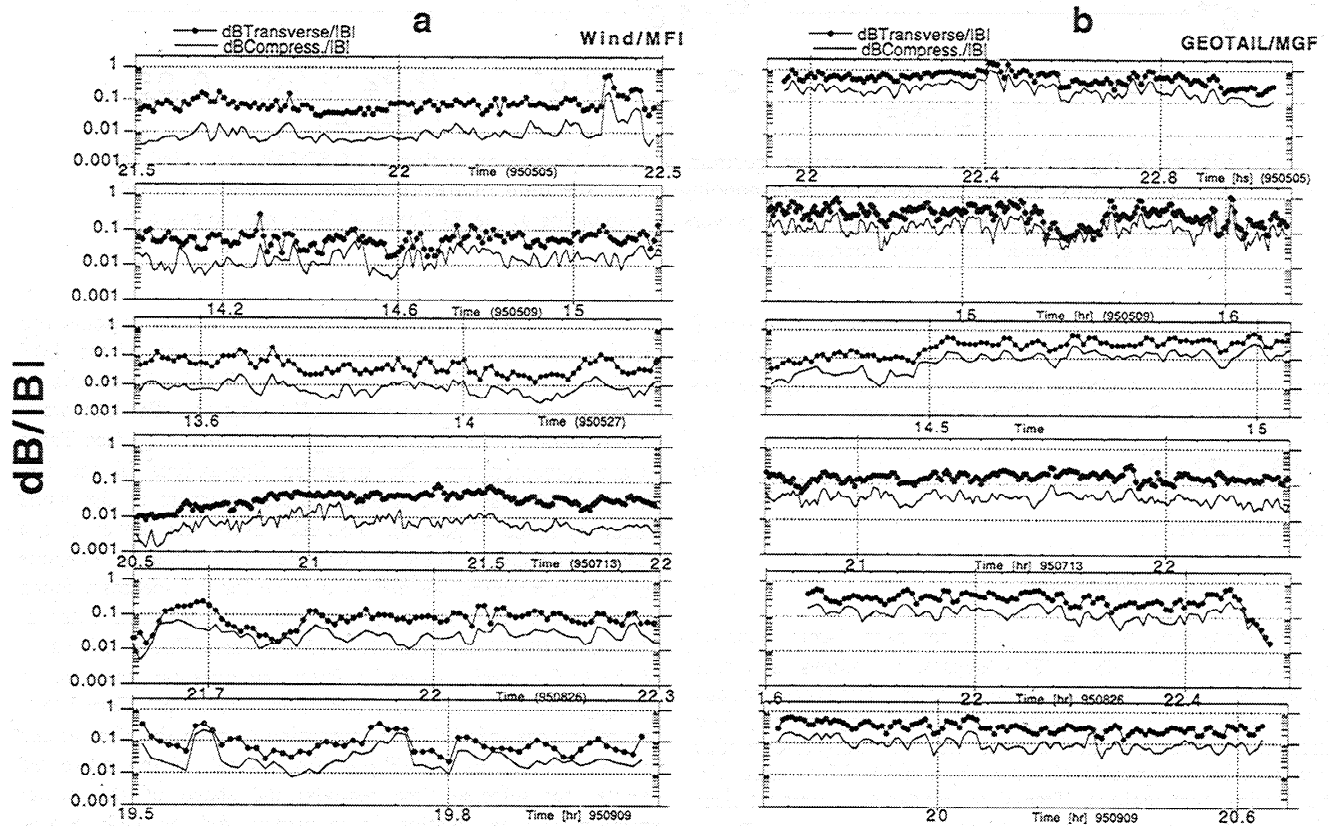

Figure 10. Figure 10a shows the ratio to the mean field <B> of the transverse ($\delta B_T = \sqrt{trace(B_\alpha B_\beta - \bar{B}_\alpha \bar{B}_\beta)}$) and compressional ($\delta B_C = \sqrt{|B|^2 - \bar{B}^2}$) IMF fluctuations observed by Wind for events 1, 2, 3, 7, 9, and 10. (Events and times are from Table 1.) Figure 10b shows the corresponding δB_T and δB_C IMF fluctuations observed by GEOTAIL for the same events.

Table 5. Partition of ULF wave activity observed in the ion foreshock

Event No.	$dB_T/|B|$ Wind	$dB_T/|B|$ GTAIL	$dB_C/|B|$ Wind	$dB_C/|B|$ GTAIL	$<f>$ Hz Wind	$<f>$ Hz GTAIL	Δf Hz Wind	Δf Hz GTAIL
1	0.085	0.62	0.013	0.27	0.018	0.023_5	0.014	0.014
2	0.061	0.36	0.018	0.15	0.014	0.019_4	0.012	0.012
3	0.051	0.375	0.008_7	0.14	0.013_5	0.021_3	0.012	0.015
4	0.052	0.29	0.010_7	0.09_2	0.022*	0.025	0.015*	0.016_5
5	0.16_{75}	0.32	0.035	0.11	0.013_3	0.017	0.012	0.011
6	0.067	0.33	0.018_4	0.11_5	0.014	0.020_5	0.012_5	0.013
7	0.034	0.17	0.008	0.043	0.032_6	0.034_4	0.023	0.021_2
8	0.076	0.23	0.017	0.06	0.019	0.024_3	0.015_5	0.017_4
9	0.092	0.35	0.040	0.13	0.019	0.023	0.016	0.013
10	0.061	0.35	0.018	0.11	0.013_3	0.018_7	0.011	0.013_2

For the ordered events (column 1) are given the average value of the ratio to the mean field $<|B|>$ of the transverse $(\delta B_T = \sqrt{trace(\overline{B_\alpha B_\beta} - \overline{B}_\alpha \overline{B}_\beta)})$ IMF fluctuations observed at Wind (column 2), and at GEOTAIL (column 3), the average value of the ratio to the mean field $<|B|>$ of the compressional $(\delta B_c = \sqrt{\overline{|B|^2} - \overline{B}^2})$ IMF fluctuations observed at Wind (column 4), and at GEOTAIL (column 5), the mean value of the ULF excitations at Wind (column 6) and at GEOTAIL (column 7), the band width of the observed excitations at Wind (column 8) and GEOTAIL (column 9).
* for interval from 1500 to 1600 UT on June 11, 1995.

the ULF wave amplitudes is conducive to the generation of the so-called plasma "firehose" instability [*Kennel and Sagdeev*, 1967; *Parker*, 1958]. This firehose instability is expected to destabilize the ULF waves in a high β plasma, generating a cascade type power spectrum with its strength concentrated in the compressional modes. The overall values of these compressional modes, however, had intensity 10-50 times weaker than the transverse modes in the observed events.

7. Ion Foreshock Observations From Both Sides of a Heliospheric Sector Boundary

The last event of Table 2 distinguishes itself from the rest of the events, because Wind and GEOTAIL were located in different heliospheric sectors of approximately opposing polarity while in the ion foreshock. Figure 11 presents the 1-min averages of the IMF for this event. The upstream IMFs, dawnward of the Earth, are given in Figures 11b and 11d, and the upstream IMFs, duskward of the Earth, Figures 11a and 11c. Figures 11a and 11b show the magnitude and the z-GSE component of the IMF, and Figures 11c and 11d the respective orientations of the IMF in the ecliptic plane.

Event 10 with an orientation of the <B> field ~ 150° apart at Wind from its orientation at GEOTAIL (see Figure 11), is unusually long lasting (~ 1 hour). This event suggests that GEOTAIL and Wind are located in the opposite sides of the current sheet. This is indicative of a possible unusual boundary between the heliospheric current sheet and the Earth's bow shock over an extended period, with the resulting development of a quasi-steady interaction state of a SW rotational or tangential discontinuity and the Earth's bow shock [*Thomsen et al.*, 1993; *Lin*, 1997]. (Both SC were several tens of RE apart; see last entry in Table 1.) Therefore it implies that the

Earth's magnetosphere had dawnward and duskward boundaries with heliospheric IMFs of nearly opposite signs for nearly an hour, i.e., conditions which may have affected its topology in unusual ways.

The method for the quantitative evaluation of the magnetic conjunction, presented in section 4, also gives a magnetic conjunction solution between Wind and GEOTAIL for event 10 but is not meaningful. This case violates the implicit assumption of one magnetic domain. In this event the SC are located in different magnetic domains of opposing polarity, i.e. different heliospheric sectors, as shown in Figure 11.

8. Conclusions

We have identified 10 intervals of simultaneous observation of fluctuating scattered (40-140 keV) energetic ions and transverse ULF wave excitations in the near and far Earth foreshock while the IMF was approximately radial from the Sun. During all these intervals the energetic ions and ULF wave enhancements which are the main signatures of the ion foreshock were observed at far away locations (up to about ~ 250 RE upstream of the Earth).

During the flappings of the magnetospheric tail, which is especially strong during the high-speed SW, the observed upstream flow of energetic ions appear to arrive from a broader region in space, i.e. beyond 30 RE from the bow shock sonic point r_{sp}. On the other hand, during more quiet intervals the location at the bow shock seemed to be within the expected limits of about 30 RE from r_{sp}.

We have presented a simple and effective method for the determination of the simultaneous and/or sequential magnetic conjunction events with the result that (1) GEOTAIL and Wind were likely connected to the same region of the ion foreshock
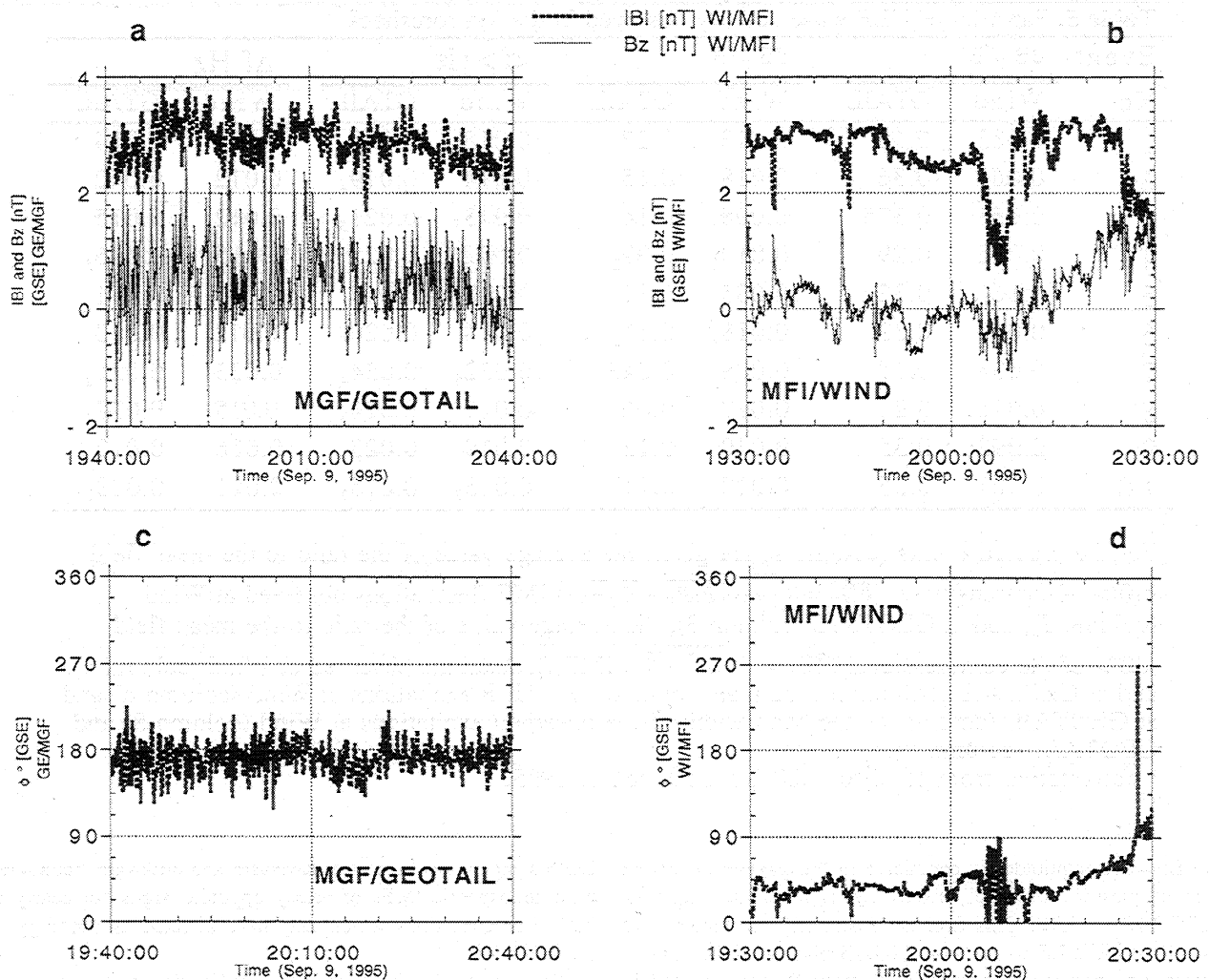
Figure 11. Example of a magnetic conjunction event with the Earth's bow shock when GEOTAIL and Wind (~ 90 RE apart) were located in different heliospheric sectors. At GEOTAIL (X-GSE, Y-GSE, Z-GSE = 6.0, -28.9, -3.9 RE) (Figure 11a) the time profile for the magnitude of the IMF and its z-GSE component are presented, and (Figure 11c) the magnitude of the azimuth angle in the [x,y-GSE] plane are presented. The corresponding IMF quantities at Wind (X-GSE, Y-GSE, Z-GSE = 82.6, 24.9, -10.9 RE) are given in Figures 11b and 11d.

for four out of the ten identified events (events 3, 4, 7, and 8), and (2) the location and time constraints were satisfied for one event (event 4) to support a possible sequential magnetic conjunction "bow shock-GEOTAIL-Wind," with a time delay between GEOTAIL and Wind of ~ 5 min, and a mean deviation $<d_{GE}> \approx 2.6$ RE from a mathematical magnetic conjunction.

This is a method of analysis of magnetic conjunction between two far-located observers in the SW. In general, it shows that for a given IMF flux line the far upstream observer (i.e., Wind) samples ULF waves and strongly scattered energetic ions earlier than the closer observer to the bow shock (i.e., GEOTAIL). This implies that in most cases GEOTAIL, which is closer to the bow shock, is also deeper in the ion foreshock in comparison with Wind. This preliminary analysis indicates that both Wind and GEOTAIL observed the same kind of ULF waves, and Wind measured a dramatic enhancement in amplitude of the ULF waves, when the IMF flux lines carried a population of strong scattered and fluctuating energetic ions. Enhanced ULF waves and fluctuating energetic ion fluxes in the same frequency range were simultaneously observed in the far

(70-250 RE upstream) and close ($\leq$ 20 RE) ion foreshock regions for all events. Far away from the bow shock, however, these ULF fluctuations appeared to have a more purely transversal nature.

The simultaneously observed energetic particles at two far locations could not belong to the same population of trapped diffused ions because our magnetic conjunction analysis indicates that in general GEOTAIL, closer to the bow shock, is deeper in the ion foreshock than Wind. They could not be the signatures of the same diffuse ion distribution sighted simultaneously by Wind and GEOTAIL between 70 and 240 RE apart because particles in the energy range discussed here will have a gyroradius of a few RE. Because of their similarities and simultaneity of observations, we interpret that the same type of coupling between ULF waves and fluctuating energetic ion fluxes was at work far from and close to the bow shock. It appears that the ULF waves may play a central role. This is suggested by our discussion in section 5 of their presence, in absence of energetic ion fluxes, while the IMF flux lines were disconnected or connected to a deep nightside region of the

bow shock. One could further investigate the possibility of the ULF waves originating farther upstream of the Earth's foreshock and being blown downstream of both spacecraft.

For one case, event 10, we have found that for an extended period (~1 hour) the magnetic field at Wind (located upstream and dawnward) is directed approximately sun-ward, while at GEOTAIL (located upstream and duskward) it is directed tailward, i.e., they are directed in opposing directions even though both Wind and GEOTAIL were located in the ion foreshock regions. These conditions imply an ion foreshock which likely (1) contains the heliospheric current sheet, and (2) causes the occurrence of unusual heliospheric boundaries to the Earth's magnetosphere over an extended period of time.

Appendix: Identification of the Magnetic Conjunction Conditions

The identification of the intervals of magnetic conjunctions reported here is the result of a systematic survey of the Wind and GEOTAIL orbits when the SC were in the SW and appeared to be magnetically connected to the Earth's bow shock along a single IMF line. For the survey we have used: (1) the orbit plots generated by tools from the "Satellite Situation Center" [*Mish et al.,* 1995], (2) the daily summary plots of key parameters from various Wind and GEOTAIL instruments, and (3) the 1-min common data format (CDF) daily files containing the key parameters of interest. In fact, this information is readily available from the science planning and operations facility (SPOF) of the international solar terrestrial physics (ISTP) program through the World Wide Web at http://www-spof .gsfc.nasa.gov/index_spof.html [*Mish et al.,* 1995; *Peredo et al.,* 1996 (available at http://www-istp.gsfc.nasa.gov/istp/ newsletter.html)]. From the orbit plots we have obtained the nominal times when both spacecraft were located in the SW and from the key parameters' plots we have obtained not only the state of the SW, but also the signatures of the possible occurrence of an event. For example, the Wind orbit information and IMF values are contained in the CDF files for the Wind/MFI key parameter data. The GEOTAIL orbit information is from the "Orbit CDF file." The Wind/MFI key parameter values were used to derive the direction of the magnetic field at Wind. By using the GSE coordinate information [e.g., *Russell,* [1971] of both SC we have estimated the distances of GEOTAIL and Earth from the direction of the IMF at Wind. We have selected those intervals where the key parameter data indicated that the IMF direction at Wind is within 20-25 RE of the GEOTAIL and the Earth position. For the most likely magnetic conjunction intervals we have examined the energetic ion flux data from the GEOTAIL/EPIC and Wind/3DP key parameters. From our list we have removed those time intervals for which the energetic ion fluxes were below background level. We have also removed those events for which the duration of the energetic ion flux enhancements lasted less than 45 minutes when Wind was at the Lagrangian point. During these events the line defined by the ray direction of the 1-min average IMF at Wind did not remain within ~ 25 RE of GEOTAIL; rather, it repeatedly wandered around the magnetic conjunction conditions. We have identified ten intervals when the (40-140 keV) energetic ion fluxes and ULF wave intensities show simultaneous enhancements in Wind and GEOTAIL particle and magnetic field data obtained from May to September 1995.

References

Asbridge, J.R., S.J. Bame, and I.B. Strong, Outward flow of protons from the earth's bow shock, *J. Geophys. Res., 73,* 5777-5782, 1968.

Bonifazi, C., and G. Moreno, Reflected and diffuse ions backstreaming from the Earth's bow shock, 1, Basic properties, *J. Geophys. Res., 86,* 4397-4404, 1981.

Burgess, D., Shock drift acceleration at low energies, *J. Geophys. Res., 92,* 1119-1130, 1987.

Eichler, D., Energetic particle spectra in finite shocks: The Earth's bow shock, *Astrophys. J., 244,* 711-716, 1981.

Ellison, D.C., E. Mobius, and G. Paschmann, Particle injection and acceleration at Earth's bow shock: Comparison of upstream and downstream events, *Astrophys. J., 352,* 376-394, 1990

Fairfield, D.H., Bowshock Associated Waves Observed in the Far Upstream Interplanetary Medium, *J. Geophys. Res., 74,* 3541-3553, 1969.

Fuselier, S.A., Ion distributions in the Earth's foreshock upstream from the bow shock, *Adv. in Space Res., 15(8/9),*43-52, 1995.

Gary, S.P., Microinstabilities upstream of the Earth's bow shock: A brief review, *J. Geophys. Res., 86,* 4331-4336, 1981.

Gosling, J.T., J.R. Asbridge, S.J. Bame, G. Paschmann, and N. Sckopke, Observations of two distinct populations of bow shock ions in the upstream solar wind, *Geophys. Res. Lett., 5,* 957-960, 1978.

Greenstadt, E.W., I.M. Green, G.T. Inouye, A.J. Hundhausen, S.J. Bame, and I.B. Strong, Correlated magnetic field and plasma observations of the Earth's bow shock, *J. Geophys. Res., 73,* 51-60, 1968.

Greenstadt, E.W., and L.W. Baum, Earth's compressional foreshock boundary revisited: observations by ISEE1 magnetometer, *J. Geophys. Res., 91,* 9001-9006, 1986.

Greenstadt, E.W., G. Le, and R.J. Strangeway, ULF waves in the foreshock, *Adv. in Space Res., 15 (8/9),* 71-84, 1995.

Harvey, C.C., M.B. Bavassano-Cattaneo, M. Dobrowolny, S. Orsini, A. Mangeney, and C.T. Russell, Correlated wave and particle observations upstream of the Earth's bow shock, *J. Geophys. Res., 86,* 4517-4529, 1981.

Ipavich, F.M., G. Gloeckler, C.Y. Fan, L.A. Fisk, D. Hovestadt, B. Klecker, J.J. O'Gallagher, and M. Scholer, Initial observations of low energy charged particles near the Earth's bow shock on ISEE-1, *Space Sci. Rev., 23(23),* 93-101, 1979.

Heppner, J.P., M. Sugiura, T.L. Skillman, B.G. Ledley, and M. Campbell, OGO-A magnetic field observations, *J. Geophys. Res., 72,* 5417-5471, 1967.

Kelly, T.J., N.U. Crooker, G.L. Siscoe, C.T. Russell, and E.J. Smith, On the use of a sunward libration-point-orbiting spacecraft as an interplanetary field monitor for magnetospheric studies, *J. Geophys. Res., 91,* 5629-5636, 1986.

Kennel, C.F., Collisionless shocks and upstream waves and particles: Introductory remarks, *J. Geophys. Res., 86,* 4325-4329, 1981.

Kennel, C.F., and R.Z. Sagdeev, Collisionless shock waves in high β plasmas, 1, *J. Geophys. Res., 72,* 3303-3326, 1967.

Kokubun, S., T. Yamamoto, M. Acuña, K. Hayashi, K. Shiokawa, and H. Kawano, The GEOTAIL magnetic field experiment, *J. Geomag. Geoelectr.*, *46*, 7-21, 1994.

Le, G., and C.T. Russell, A study of ULF wave foreshock morphology, I, ULF foreshock boundary, *Planet. Space Sci.*, *40*, 1203-1213, 1992.

Lee, M.A., Coupled hydromagnetic wave excitation and ions acceleration upstream of the Earth's bow shock, *J. Geophys. Res.*, *87*, 5063-5080, 1982.

Lepping, R.P., et al., The Wind magnetic field investigation, *Space Sci. Rev.*, *71*, 207-229, 1995.

Lin, R.P., C.-I. Meng, and K.A. Anderson, 30- to 100-keV Protons upstream from the Earth's bow shock, *J. Geophys. Res.*, *79*, 489-498, 1974.

Lin, R.P., et. al., A Three-dimensional plasma and energetic particle investigation for the Wind spacecraft, *Space Sci. Rev.*, *71*, 125-153, 1995.

Lin, Y., Generation of anomalous flows near the bow shock by its interaction with interplanetary discontinuities, *J. Geophys. Res.*, *102*, 24265-24381, 1997.

Mish, W.H., J.L. Green, M.G. Reph, and M. Peredo, ISTP science data systems and products, *Space Sci. Rev.*, *71*, 815-878, 1995.

Mitchell, D.G., E.C. Roelof, T.R. Sanderson, R. Reinhard, and K.-P. Wenzel, ISEE/IMP Observations of simultaneous upstream ion events, *J. Geophys. Res.*, *88*, 5635-5644, 1983.

Ogilvie, K.W., et al., SWE, A comprehensive plasma instrument for the Wind spacecraft, *Space Sci. Rev.*, *71*, 55-77, 1995.

Parker, E.N., Dynamical instability in an anisotropic ionized gas of low density, *Phys. Rev.*, *109*, 1874-1876, 1958.

Paschmann, G., N. Sckopke, S.J. Bame, J.R. Asbridge, J.T. Gosling, C.T. Russell, and E.W. Greesntadt, Association of low-frequency waves with suprathermal ions in the upstream solar wind, *Geophys. Res. Lett.*, *6*, 209-212, 1979.

Peredo, M., J.A. Slavin, E. Mazur, and S. A. Curtis, Three-dimensional position and shape of the bow shock and their variation with Alfvenic, sonic and magnetosonic Mach numbers and interplanetary magnetic field orientation, *J. Geophys. Res.*, *100*, 7907-7916, 1995.

Peredo, M., S. Boardsen, D. Berdichevsky, and G. Galiardi, New ISTP products on the SPOF World Wide Web Server, *ISTP Newsl.*, *6(2)*, 33-34, 1996.

Russell, C.T., Geophysical coordinate transformations, *Cosmic Electro-Dyn.*, *2*, 184-196, 1971.

Russell, C.T., G.L. Siscoe, and E.J. Smith, Comparison of ISEE-1 and -3 interplanetary magnetic field observations, *Geophys. Res. Lett.*, *7*, 381-384, 1980.

Sanderson, T.R., R. Reinhard, and K.-P. Wenzel, The Propagation of Upstream Protons Between the Earth's Bowshock and ISEE-3, *J. Geophys. Res.*, *86*, 4425-4434, 1981.

Slavin, J.A., R.E. Holzer, J.R. Spreiter, and S.S. Stahara, Planetary Mach Cones: Theory and Observation, *J. Geophys. Res.*, *89*, 2708-2714, 1984.

Scholer, M., F.M. Ipavich, G. Gloeckler, D. Hoverstadt, and B. Klerker, Upstream particle events close to the bow shock and 200 RE upstream: ISEE-1 and ISEE-3 observations, *Geophys. Res. Lett.*, *7*, 73-76, 1980.

Scholer, M., G. Gloeckler, F.M. Ipavich, D. Hovestadt, and B. Klecker, Pitch angle distributions of energetic protons near the Earth's bow shock, *Geophys. Res. Lett.*, *6*, 707-710, 1979.

Sonnerup, B.U.O., and Cahill, L.J. Jr., Magnetopause structure and attitude from Explorer 12 observations, *J. Geophys. Res.*, *72*, 171-183, 1967.

Terasawa, T., Origin of 30-100 keV Protons observed in the upstream region of the Earth's bow shock, *Planet. Space Sci.*, *27*, 365-384, 1979.

Thomsen, M.F., V.A. Thomas, D. Winske, J.T. Gosling, M.H. Farris, and C.T. Russell, Observational test of hot flow anomaly formation by the interaction of magnetic discontinuity with the bow shock, *J. Geophys. Res.*, *98*, 15,319-15,330, 1993.

Williams, D.J., R.W. McEntire, C. Schlemm II, A.T.Y. Lui, G. Gloeckler, S.P. Christon, and F. Gliem, GEOTAIL energetic particles and ion composition instrument, *J. Geomagn. Geoelectr.*, *46*, 39-57, 1994

D. Berdichevsky, Raytheon-STX Corporation, at NASA/GSFC, Greenbelt, MD 20771, email: berdi@istp1.gsfc.nasa.gov

R. Fitzenreiter and R. Lepping, NASA/GSFC, Greenbelt, MD 20771

S. Kokobun, Solar-Terrestrial Environment Laboratory, Nagoya University, Toyokawa, Aichi 442, Japan

R.P. Lin, Dept. of Phys., Univ. of California, Berkeley, CA

R. McEntire and D. Williams, JHU/ Applied Physics Laboratory, Laurel, MD

G. Thejappa, Dept. of Astr., Univ. of Maryland, College Park, MD 20742

T. Yamamoto, Institute of Space and Astronautical Science, Sagamihara, Kanagawa 229, Japan